Chemical Geology 389 (2014) 29–47

Contents lists available at ScienceDirect

Chemical Geology

journal homepage: www.elsevier.com/locate/chemgeo

Geochemistry of Alpine serpentinites from rifting to subduction: A view across paleogeographic domains and metamorphic grade

Jaime D. Barnes [a,*], Marco Beltrando [b], Cin-Ty A. Lee [c], Miguel Cisneros [a], Staci Loewy [a], Emily Chin [c]

[a] Department of Geological Sciences, University of Texas, Austin, TX 78712, USA
[b] Dipartimento di Scienze della Terra, Università di Torino, Via Valperga Caluso 35, 10125 Torino, Italy
[c] Department of Earth Science, MS-126, Rice University, Houston, TX 77005, USA

ARTICLE INFO

Article history:
Received 21 April 2014
Received in revised form 11 September 2014
Accepted 14 September 2014
Available online 28 September 2014

Editor: L. Reisberg

Keywords:
Serpentinite
Alps
Stable isotope geochemistry
Trace element geochemistry

ABSTRACT

Serpentinites from several tectono-metamorphic units of the Western Alps were studied to constrain their origin and tectonic setting of serpentinization. Study areas were selected to cover the whole width of the orogen and a wide range of metamorphic grades from anchizone (Canavese Zone) to greenschist facies (St. Barthelemy, Piemonte Zone) to blueschist facies (Rocca Canavese unit and Punta Rossa unit). Bulk rock serpentinite samples have high REE concentrations, compared to typical mid-ocean ridge serpentinites, with nearly flat REE patterns. Relict spinels from the Rocca Canavese unit have extremely low Cr#s (average = 0.087) and high Mg#s (average = 0.798) suggesting very low degrees of melt depletion. Both of these observations are consistent with an abyssal origin in a hyper-extended rifted margin with minimal melt depletion, or refertilization. Seafloor hydration between 150 and 200 °C is indicated by oxygen isotope data ($\delta^{18}O$ values = +5.2 to + 9.4‰), supporting lithostratigraphic evidence of exhumation to the floor of the Alpine Tethys already available for the Canavese, St. Barthelemy and Punta Rossa serpentinites. Subsequent interaction with the metasediments during Alpine metamorphism resulted in variations in trace element concentrations and stable isotope compositions with decreasing distance to the interface between the sediment and serpentinite. The chemical gradient between the ultramafic rocks and the neighboring metasediments is best seen in the Punta Rossa unit, where Pb, Ba, Cs, U, and Rb concentrations increase, $\delta^{18}O$ values increase, $\delta^{37}Cl$ values decrease within the serpentinite with decreasing distance to the contact and a "blackwall" of pure chlorite is found at the contact. As these contacts between ultramafic rocks, continental basement and meta-sediments are analogous to the slab–mantle interface, our results support the mobility of Pb, Ba, Cs, U, Rb, Cl, and water at the scale of <10 m across the interface during Alpine metamorphism. However, the preservation of geochemical gradients within the Punta Rossa serpentinite indicates a limited role for externally derived fluid flux.

1. Introduction

Serpentinites are a major constituent of fossil subduction zones preserved in orogens, such as the Western Alps. Within tectonometamorphic units that recorded high pressure metamorphic conditions, serpentinites are juxtaposed with a variety of rock types, ranging from meta-pillow basalts, meta-gabbros, syn- to post-rift metasedimentary sequences to continental basement rocks and pre-rift metasediments (e.g., Bodinier and Godard, 2005; Beltrando et al., 2014). Lithological interfaces between serpentinites and the neighboring rocks are often defined by reaction rims, indicative of extensive metasomatism (e.g., Dal Piaz, 1967; Malvoisin et al., 2012; Galvez et al., 2013; Vitale Brovarone et al., 2014). Controversies as to the origin of the serpentinites and the tectonic environment of juxtaposition with the now adjacent rocks lie at the base of radically different views on subduction/exhumation dynamics. Serpentinites from the high pressure part of the Alpine belt are alternately viewed as having originated mostly from the now subducted Alpine Tethys, which was largely floored by exhumed mantle peridotites in a hyper-extended rifted margin (Dal Piaz, 1999; Manatschal and Müntener, 2009; Beltrando et al., 2014), from the hydrated mantle wedge (e.g., Schwartz et al., 2001; Gerya et al., 2002) or from a combination of both (e.g., Guillot et al., 2009; Malatesta et al., 2012).

In the context of this debate, field-based studies performed in several high-pressure tectonometamorphic units in the Western Alps and Corsica have commonly documented the local preservation of rift-related associations consisting of serpentinites and syn- to post-rift sediments (e.g., Dal Piaz, 1969; Lemoine et al., 1970; Elter, 1971; Lagabrielle et al., 1982; Tricart and Lemoine, 1983), occasionally juxtaposed with continental basement allochthons (Dal Piaz, 1999; Beltrando et al., 2010a, 2012; Vitale Brovarone et al., 2011). These lithological associations are comparable to the well-preserved examples from the little deformed/metamorphosed Eastern Alps in the Engadine and Graubunden regions (Switzerland), where pre-Alpine structures and basement-

* Corresponding author.
E-mail address: jdbarnes@jsg.utexas.edu (J.D. Barnes).

http://dx.doi.org/10.1016/j.chemgeo.2014.09.012
0009-2541/

sedimentary cover relationships characteristic of magma-poor rifted margins of the kind presently found in the Northern Atlantic are exposed (e.g., Afilhado et al., 2008; e.g., Froitzheim and Eberli, 1990; Froitzheim and Manatschal, 1996; Manatschal, 2004; Manatschal and Müntener, 2009; Mohn et al., 2010; Peron-Pinvidic and Manatschal, 2009). However, the ability to structurally constrain the origin of mantle peridotites is highly dependent on the extent of subduction/orogeny related reworking of lithological contacts and on outcropping conditions (see discussion in Beltrando et al., 2014). In this study, the ability of Alpine serpentinites to retain traces of their origins is explored with a detailed geochemical study, to provide an additional tool to decipher the origin of the protolith and the fluid responsible (and hence location) for serpentinization.

Additionally, since the lithological associations studied here, consisting of serpentinites, meta-sediments, and continental basement, together with the associated metasomatism during subduction zone metamorphism may be analogous to the subducting slab-serpentinized mantle wedge interface, these contacts can also be used to study chemical exchange between subducting rocks and the mantle wedge, assuming that the sediment contact within the slab is undergoing dehydration. Much work has focused on the nature of this slab–mantle interface and the elemental transfer across this zone (e.g., see reviews in Bebout, 2007; Bebout, 2012). Subducting altered oceanic crust and sediments are the main potential sources of LILE (e.g., Ba, K, Rb, Cs, Sr), U and P to subduction zone fluids (e.g., Hawkesworth et al., 1993; Plank and Langmuir, 1993; Bebout et al., 1999; Scambelluri and Philippot, 2001; Breeding et al., 2004; Spandler et al., 2004). Serpentinites are a "sponge" for volatile and fluid-mobile elements (FME) (e.g., Cl, F, B, S, As, Sb, Pb) and play a central role in the recycling of these elements during subduction (e.g., Anselmi et al., 2000; Hattori and Guillot, 2003, 2007; Straub and Layne, 2003; Scambelluri et al., 2004; Sharp and Barnes, 2004; Barnes and Sharp, 2006; Agranier et al., 2007; Vils et al., 2008; Deschamps et al., 2011; Kodolányi et al., 2012). Forearc wedge serpentinites are notably enriched in FME, compared to abyssal peridotites (Hattori and Guillot, 2003, 2007; Savov et al., 2005, 2007; Deschamps et al., 2010; Kodolányi et al., 2012), and may be dragged to sub-arc depths influencing the composition of arc magmatism (Hattori and Guillot, 2003; Straub and Layne, 2003). In this study, we are particularly interested in the role of serpentinite as a host for FME during elemental transfer from the sediment to the mantle and the depth to which serpentinites retain their FME budget.

Here we present the first geochemical data for serpentinites from four different tectono-metamorphic units in the Western Alps: 1) the Punta Rossa unit (Internal Valaisan domain) near the Petit St. Bernard Pass (Loprieno et al., 2011; Beltrando et al., 2012); 2) the Combin Zone, which is part of the Piemonte units, in the vicinity of the village of St. Barthelemy (Aosta Valley); 3) the Rocca Canavese unit, at the SW termination of the Sesia Zone and 4) the Canavese Zone, between the villages of Levone and Rivara (Beltrando et al., in press) (Fig. 1). These localities were selected in order to provide the widest coverage in terms of paleogeographic origin of the different units and present day position within the Alpine belt, from the Periadriatic Line to the Penninic Front. Previous studies showed that the Punta Rossa (Beltrando et al., 2012), St. Barthelemy (Baldelli et al., 1983), and Canavese Zone serpentinites (Elter et al., 1966; Beltrando et al., in press) were exhumed at the floor of the Western Tethys; whereas, the origin of the Rocca Canavese unit serpentinites is ill defined, partly due to the rather poor exposure available (Pognante, 1989). We use major and trace elements and stable isotope geochemistry to complement existing structural and lithostratigraphic data to decipher the serpentinization and tectonic history of these highly deformed metamorphic units, as well as, trace the geochemical modification of serpentinites due to interaction with sedimentary-derived fluids. These areas provide an opportunity to trace multi-stage serpentinization of abyssal peridotites from the Jurassic ocean-continent transition throughout Alpine metamorphism.

2. Geologic setting

2.1. Geology of the Western Alps

Late Cretaceous to Early Tertiary convergence between the Adriatic and Eurasian plates resulted in the closure of the intervening Tethyan ocean basin, culminating in continent–continent collision at the Eocene–Oligocene boundary (see Beltrando et al., 2010b for a review; Coward and Dietrich, 1989; Dewey et al., 1973). The Western Alps can be subdivided into three major domains: 1) Southern Alps; 2) Axial Belt; 3) External Zone (Fig. 1). 1) The Southern Alps (located on the Adriatic plate) comprise Permian continental basement overlain by Permian volcanic rocks and Meso/Cenozoic sediments. Alpine deformation and metamorphism are relatively minor and mostly limited to the vicinity of the Periadriatic Line. 2) The Axial Belt is bounded by the Periadriatic Line and Penninic Front. It consists of tectono-metamorphic units that originated from both the Adriatic and European continental margins and from the Western Tethys Ocean, where mantle exhumation occurred in the Middle to Upper Jurassic (e.g., Bill et al., 2001). The Western Tethys consisted of two main branches, commonly referred to as Piemonte–Ligurian (or South Penninic) and Valaisan Basins (or North Penninic) (Frisch, 1979; Trümpy, 1980). The axial belt is commonly subdivided into the "Austroalpine Units", mainly consisting of Paleozoic continental basement and minor Mesozoic meta-sediments originated from the distal Adriatic margin (Pognante, 1989; Beltrando et al., 2014), and "Penninic units." The latter comprise units derived from the European margin and the Tethys Ocean. These terranes underwent Alpine metamorphism ranging from greenschist facies to UHP eclogite facies conditions (see Beltrando et al., 2010b; Dal Piaz, 2010; Rosenbaum and Lister, 2005 for recent reviews). 3) The External Zone is a nappe stack resting on the European plate, which underwent low grade Alpine metamorphism.

2.2. Serpentinites of the Western Alps

Western Alpine ultramafic bodies largely originated from the Alpine Tethys ocean basin (Manatschal and Müntener, 2009). Several Tethyan peridotites preserve the record of a complex pre-orogenic history suggestive of multi-stage lithospheric thinning, ultimately culminating in exhumation to the basin floor (e.g., Li et al., 2004; Groppo and Compagnoni, 2007). Progressive early exhumation from garnet to spinel facies depths was commonly followed by melt impregnation at spinel and plagioclase facies conditions, prior to serpentinization (see Piccardo, 2010 for a review). This evolution has been best documented in the Lanzo massif (e.g., Müntener and Piccardo, 2003; Piccardo et al., 2007; Debret et al., 2013) and Erro-Tobbio peridotites from the Piemonte units (e.g., Rampone and Borghini, 2008).

Serpentinized peridotites from the Piemonte units and Lanzo massif largely underwent blueschist to eclogite facies Alpine metamorphism. Serpentinization is generally attributed to seafloor hydration, although alternate interpretations include subduction-related processes, such as hydration of mantle wedge peridotites (Schwartz et al., 2001; Gerya et al., 2002; Federico et al., 2007) resulting in buoyancy-driven return flow of HP rocks in a serpentinite channel. Pervasive subduction-related deformation and metamorphism complicate the assessment of the pre-Alpine relationships between serpentinites and surrounding rocks. Despite these difficulties, observations from specific parts of the Western Alps suggest that several ultramafic bodies were exhumed at the basin floor in the Jurassic (e.g., Elter et al., 1966; Lemoine et al., 1970; Lagabrielle et al., 1982; Dal Piaz, 1999, 2010; Beltrando et al., 2010a, 2012; Manatschal et al., 2011), although it is still unclear to what extent mantle serpentinization took place at the basin floor as opposed to during subduction and orogeny.

Other occurrences of serpentinites are located in the proximity of the Insubric Line, both in the Canavese Zone (Elter et al., 1966), which underwent very low temperature metamorphism, and in the Rocca

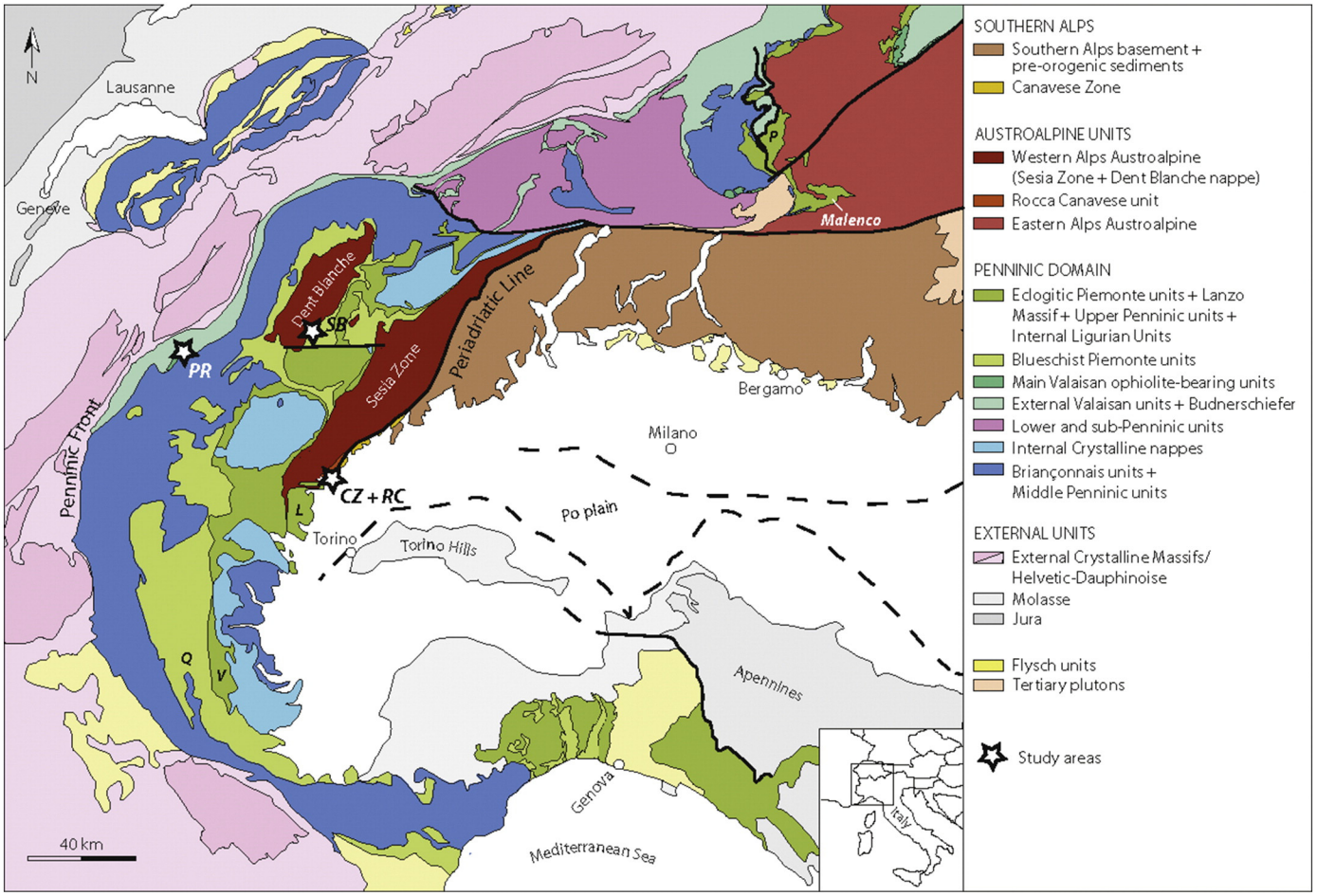

Fig. 1. Tectonic map of the Western Alps. Stars highlight the Punta Rossa (PR) unit, the Combin Zone near St. Barthelemy (SB), the Rocca Canavese (RC) unit, and the Canavese Zone (CZ), near the Levone River sequence. Also noted are the Platta (P) and Malenco ultramafic bodies for reference. L: Lanzo massif; Q: Queiras; V: Monviso.

Canavese unit, which was buried to lawsonite–blueschist facies conditions (Pognante, 1989) and along the tectonic lineament itself (e.g., Ferrando et al., 2004). In the more external Valaisan domain, serpentinized sub-continental mantle is found associated with continental basement and Mesozoic meta-sediments (Masson, 2002; Loprieno et al., 2011; Beltrando et al., 2012).

2.2.1. Punta Rossa unit, Petit St. Bernard Pass, Internal Valaisan domain

The Punta Rossa unit crops out in the Internal Valaisan domain, near the Petit St. Bernard Pass (French-Italian border) (Figs. 1 and 2). This tectonometamorphic unit samples remnants of the Valaisan basin, which separated the Briançonnais continental ribbon from the European plate sensu stricto (e.g., Trümpy, 1980; Beltrando et al., 2007). As shown by Beltrando et al. (2012), the Punta Rossa unit preserves evidence of mantle exhumation at the seafloor during Tethyan rifting. Serpentinites are juxtaposed with slivers of continental basement or coarse meta-sedimentary breccia (Fig. 3A and B). The contacts between the serpentinites and basement are interpreted as Mesozoic detachment faults that have been preserved locally despite Alpine deformation. All of the above lithologies are then overlain by post-rift pelagic sediments, including radiolaria-bearing micaschists (Beltrando et al., 2012). Early stage Alpine metamorphism ($P \approx 1.7$ GPa; $T \approx 375$ °C) was followed by exhumation, possibly accompanied by minor reheating (Bousquet et al., 2002; Beltrando et al., 2012). Evidence of syn-metamorphic interaction between serpentinites and continental basement is indicated by metasomatic rims, ranging in thickness from a few dm to over 2 m, and largely consisting of tremolite, talc and carbonate. Massive chlorite–actinolite schists are also found in this position.

2.2.2. Combin unit at St. Barthelemy (Piemonte units)

The ophiolite-bearing tectono-metamorphic units cropping out to the north of the Aosta Ranzola fault and sandwiched inbetween the underlying Eclogitic Piemonte units and the overlying Austroalpine units are grouped under the common label of 'Combin unit' (Bearth, 1967). They consist predominantly of a thick sequence of meta-marls, micaschists and impure marble, referred to as 'calcschists' in the Alpine literature, intercalated with slivers of serpentinites, ophicalcites and meta-mafic rocks. Mn-rich meta-cherts are commonly found at the interface between serpentinites or meta-mafic rocks and the neighboring calcschists (Carta Geologica d'Italia/APAT, S.G., 2006; Dal Piaz, 2010). This specific rock type, within the fossil Alpine Tethys realm, is considered as the metamorphic equivalent of the Mn-rich radiolarian cherts deposited directly onto exhumed mantle in seafloor position (see Dal Piaz, 2010).

An overturned contact between exhumed serpentinites and Mn-rich meta-sediments crops out near the village of St. Barthelemy, in the immediate footwall of the Austroalpine units (Baldelli et al., 1983). There massive serpentinites are locally underlain by ophicalcites. The latter are then in contact with a complex meta-sedimentary sequence, mostly consisting of quartzites and quartzitic schists interlayered with pelitic schists and marbles, hosting Mn-rich lenses, mainly consisting of braunite ($Mn^{2+}Mn^{3+}{}_6SiO_{12}$) (Baldelli et al., 1983). Preserved Alpine

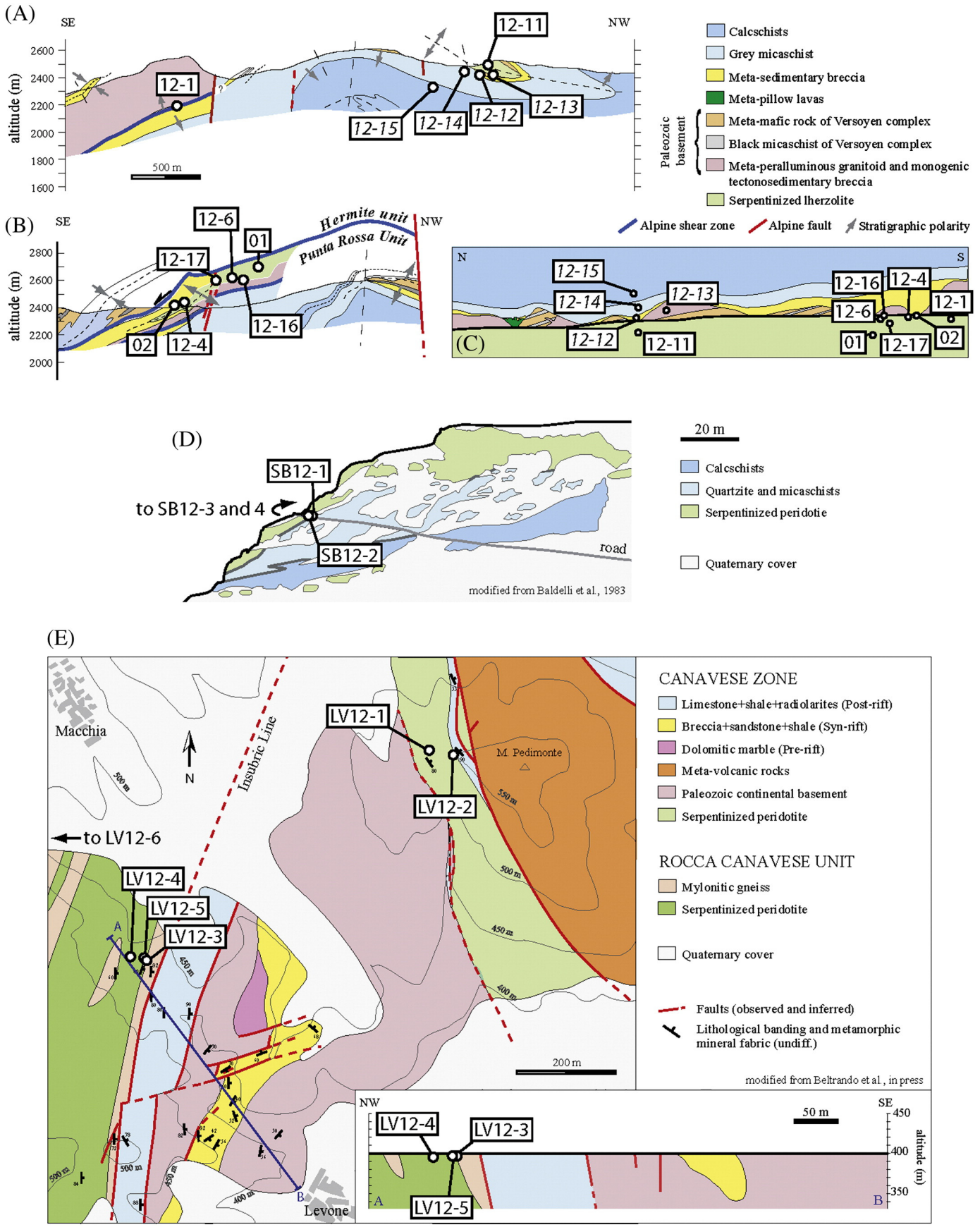

Fig. 2. Geological maps and cross sections of the study areas. A) and B) Cross section of the Punta Rossa unit showing locations of samples analyzed in this study (modified from Beltrando et al., 2012). C) Reconstructed cross section illustrating estimated distances to the continental basement/metasedimentary unit. (See Fig. 3 in Beltrando et al., 2012 for location of cross sections.) D) Panoramic view of the Saint Barthelemy sequence (modified from Baldelli et al. (1983); E) simplified geological map of the southern Canavese Zone and the adjacent Rocca Canavese unit, near the village of Levone. The cross section is drawn along the Levone river valley (modified from Beltrando et al., in press).

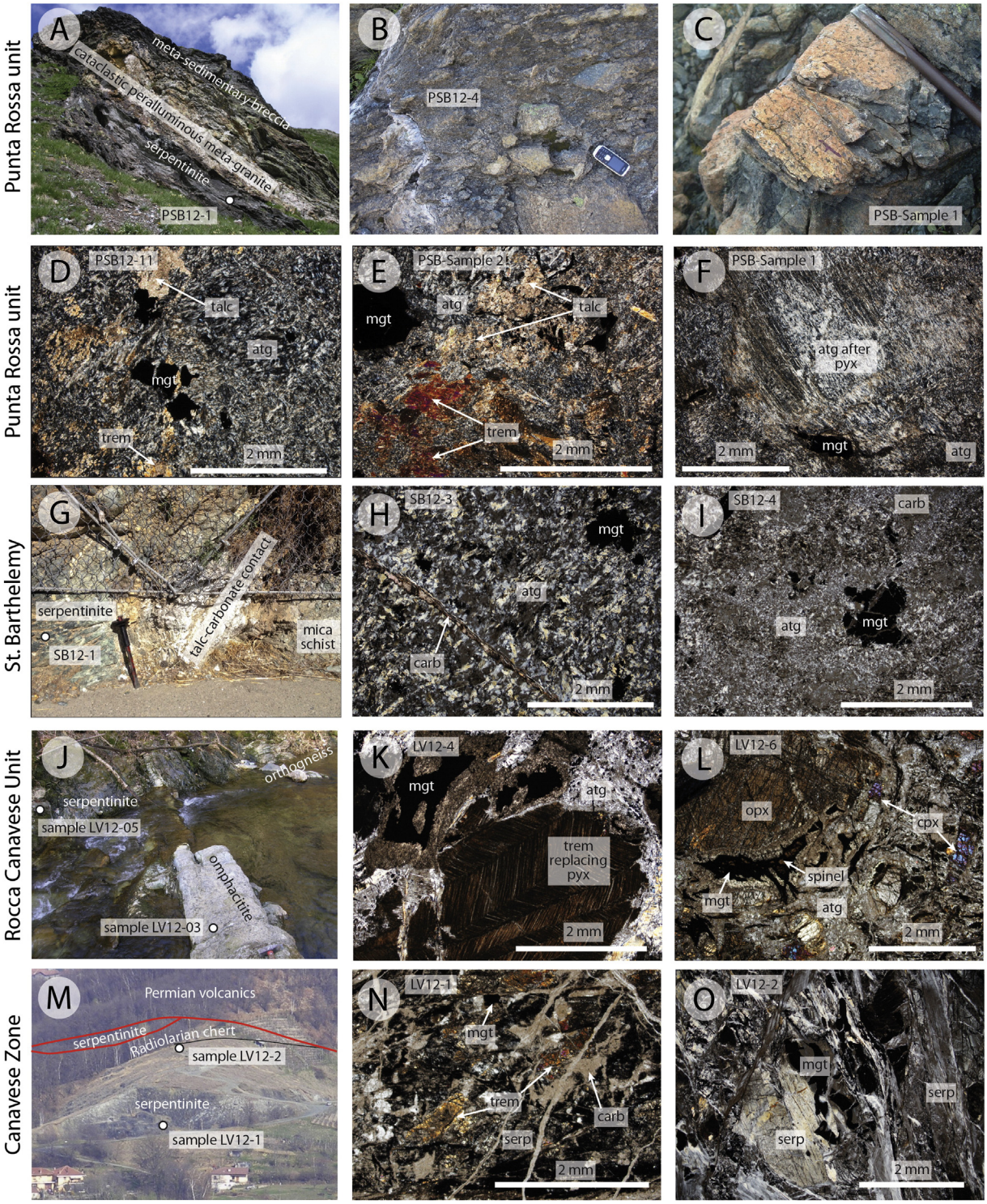

Fig. 3. Field and thin section photographs. A) Foliated serpentinite sample PSB12-1 located < 2 m from the contact with Paleozoic continental basement overlain by meta-sedimentary breccia; B) Cataclastic serpentinite sample PSB12-4 located < 2 m from the contact with the metasediments; C) Massive serpentinite sample PSB-Sample 1 located 15–20 m from the contact with metasediments; D) PSB12-11 located 10–15 m from the contact with metasediments, containing antigorite, magnetite, talc, and tremolite (trem); E) PSB-Sample2 located < 2 m from the contact with metasediments and containing antigorite, magnetite, talc, and tremolite (talc and tremolite increase in modal abundance closer to the contact); F) PSB-Sample 1 consisting of magnetite (mgt) and antigorite (atg) after pyroxene (pyx) and olivine; G) serpentinite (sample SB12-1 shown) adjacent to mica schist near the town of St. Barthelemy; a highly brecciated talc-carbonated zone lies at the contact between the two different rock types; H) SB12-3 located 20 m from the contact containing fine-grained antigorite, magnetite, and carbonate veins; I) SB12-4 located 40 m from the contact containing very fine-grained antigorite, magnetite, and patchy carbonate; J) massive serpentinite sample LV12-5 located < 1 m from the contact with the orthogneiss; the contact is defined by an omphacitite (LV12-3); K) LV12-4 showing antigorite and magnetite with twinned pyroxene replaced by tremolite; L) LV12-6 showing relict clinopyroxene (cpx), orthopyroxene (opx), and spinel; spinel is rimmed by magnetite and antigorite defines the groundmass; M) samples LV12-1 and LV12-2 are capped by radiolarian chert; N) LV12-1 showing serpentine and magnetite cross-cut by numerous carbonate veins and pyroxene altering to tremolite; O) highly sheared LV12-2 (all thin section photographs are in cross-polarized light).

mineral assemblages are indicative of greenschist facies metamorphic conditions, with rare relics of Na-amphibole and chloritoid possibly indicating pre-existing re-equilibration at blueschist facies conditions (Baldelli et al., 1983).

2.2.3. Rocca Canavese Unit (Sesia Zone)

The Rocca Canavese Unit (RCU) crops out at the SE termination of the Sesia Zone. It is bounded to the SE by the Periadriatic Line, separating it from the Canavese Zone. The SW termination of the RCU is covered by Quaternary sediments (Spalla and Zulbati, 2003). To the NW, the Rocca Canavese Zone is separated from the rest of the Sesia Zone by a blueschist facies shear zone (Spalla and Zulbati, 2003). The RCU was first defined by Pognante (1989) as an assembly of different thrust sheets alternately consisting of variably serpentinized mantle peridotites, pre-Alpine granulites, glaucophanic schists, leucocratic gneiss and minor marbles. Lawsonite-bearing blueschist facies mineral fabrics are widely preserved and generally oriented sub-parallel to the steeply dipping NE–SW trending Periadriatic Line. Serpentinites are found in several bodies ranging in thickness from a few meters to hundreds of meters. Relict minerals of the original lherzolite assemblage are locally preserved, especially in the core of the largest bodies. Static (no evidence of deformation) serpentinization becomes more and more pervasive towards the contact with the surrounding gneiss. Within the last few meters from the lithological interface, the original mantle peridotite textures are replaced by massive and foliated serpentinites. Metasomatic reaction rims are locally found at the contact between serpentinites and surrounding gneisses, both along the Levone river section (Beltrando et al., in press), to the NE of Rocca Canavese and along the Fandaglia stream (Spalla and Zulbati, 2003). The common presence of omphacite within these reaction zones indicates that the juxtaposition of serpentinites and surrounding gneisses dates back to the oldest Alpine recrystallization stages preserved in the area. To our knowledge, the RCU serpentinites have never been the target of previous geochemical studies.

2.2.4. Canavese Zone

The Canavese Zone crops out at the western edge of the Southern Alps, in the proximity of the Periadriatic Line. It is bounded to the SE by the so-called Internal Canavese Line (Biino and Compagnoni, 1989) and to the NW by the Periadriatic Line itself. This tectono-metamorphic unit samples different parts of the distal Adriatic margin, where rift-related thinning locally led to the exhumation of mantle peridotites to the seafloor (Elter et al., 1966; Ferrando et al., 2004). The largest hydrated peridotite crops out at the southern end of the Canavese Zone, near the village of Levone, where a NW–SE trending serpentinite sliver is found directly in contact with radiolarian cherts, considered to be early-post-rift sediments (Elter et al., 1966; Beltrando et al., in press). A core-to-rim zoning is observed within this serpentinite sliver, with sub-cm thick pyroxenitic dikes still visible within the core, then grading towards a massive serpentinite and serpentinite schists towards the edges. NE–SW trending faults bound the Pesmonte serpentinite on both sides (Beltrando et al., in press).

3. Sample description

3.1. Punta Rossa unit, Petit St. Bernard Pass, Internal Valaisan domain

The two largest serpentinite outcrops are located in the southern part of the Breuil valley, near Punta Rossa peak, and in the central part, near Tormottaz lake (Beltrando et al., 2012). Most serpentinite samples were collected from the first locality, where serpentinites crop out at the core of an isoclinal synformal structure, related to early-exhumation deformation, locally affected by late-stage NE–SW trending normal faults (Fig. 2) (Beltrando et al., 2012). The serpentinites were sampled at increasing distances (~1 m to ~40 m) from the contact with continental basement and/or metasedimentary units (Table 1). Distances were determined by reconstructed cross-sections (Fig. 2). We note that PSB12-17 is located between two late faults. One serpentinite sample (PSB12-11) near Tormottaz lake was sampled for comparison with samples closer to the Punta Rossa peak (Fig. 2). In addition, four representative samples of the different rock types cropping out in proximity of the serpentinite were analyzed: Permian leucogranite affected by rift-related cataclastic deformation (PSB12-13), tectono-sedimentary breccia (PSB12-12), gray mica schist (PSB12-14) and calc-schist (PSB12-15). A massive chlorite schist (PSB12-16) from the interface of the serpentinites and underlying Paleozoic basement was also collected.

All ultramafic rocks are completely serpentinized and now consist primarily of antigorite and minor magnetite. Antigorite was identified as the primary serpentine polymorph by XRD using the Bruker D8 Advance X-Ray Diffractometer at the University of Texas at Austin. Distinguishing antigorite from lizardite via XRD is difficult. Antigorite was identified by two means: 1) a broader peak and higher intensity of peaks at ~35.3 °2θ (indicative of antigorite) and 2) a lower figure of merit (best fit) for antigorite, relative to lizardite, as suggested by the program EVA. LOI wt.% losses are also consistent with XRD scans and suggest that antigorite is the primary serpentine polymorph. Tremolite, talc, and rare carbonate are also present in some samples (PSB12-1, PSB12-4, PSB12-11, PSB12-17, PSB12-Sample2) (Table 1; Fig. 3D and E). In general, the percentage of talc increases closer to the contact with basement and/or metasediment (Fig. 3D and E); however, there are some exceptions. For example, sample PSB12-6, ~2 m from the contact, contains no talc. Serpentinites further from the contact still maintain pseudomorphic textures, e.g., bastite in PSB12-Sample1 (Fig. 3F), and become increasingly sheared or display fine-grained interlocking antigorite near the contact.

3.2. St. Barthelemy

Samples SB12-1, SB12-2, SB12-3, and SB12-4 are all massive serpentinites. Sample SB12-1 is located within 2 m of the contact with mica schists and calc-schists, in a transitional area between serpentinite and meta-sediments hosting minor faults. The contact between the serpentinites and the metasediments is defined by a ~0.5 meter thick talc-carbonate layer (Fig. 3G). All serpentinites are completely serpentinized to antigorite and magnetite with no preservation of mantle textures. All antigorite is fine-grained and interlocking (Fig. 3H and I). No relict grains of the original peridotite assemblage are preserved. Carbonate is present in varying amounts in all four SB serpentinite samples (Table 1; Fig. 3H and I).

3.3. Rocca Canavese Zone

Samples LV12-3 to LV12-5 were collected from the SE end of the Rocca Canavese unit, within 50 m from the Periadriatic Line, along the banks of the Levone river. LV12-3 is a metasomatic rim consisting solely of omphacite at the contact between the serpentinite and orthogneiss (Fig. 3J). LV12-5 is a massive serpentinite ~50 cm from the omphacite. Serpentinite LV12-4 was collected ca. 30 m upstream from LV12-5 and preserves evidence of the mantle peridotite texture in hand sample. LV12-6 was collected from the SW slope of the Levone river, near the Bal windmill, >150 m away from any contact with the Paleozoic basement. LV12-4, LV12-5, and LV12-6 all contain antigorite (determined by XRD). LV12-4 and LV12-5 are completely serpentinized to antigorite and magnetite. Pyroxene is replaced by tremolite (Fig. 3K). LV12-6 is the only sample in the study that contains relict orthopyroxene, clinopyroxene, and spinel (Table 1; Fig. 3L). Spinel altering to magnetite and antigorite makes up the groundmass of the sample (Fig. 3L).

3.4. Canavese Zone

LV12-1 and LV12-2 are from the Canavese Zone. LV12-1 is a massive serpentinite located 30–40 m from radiolarian chert and Paleozoic

Table 1
Sample descriptions and localities.

Sample	Latitude/Longitude	Distance for contact with basement/ metasediments (m)	Description	Mineralogy
Punta Rossa unit (Petite St. Bernard Pass)				
Serpentinites				
PSB12-1	N 45°41′55.75″/E 6°51′35.16″	<2	Foliated serpentinite	Antigorite + talc + mgt
PSB12-4	N 45°41′45.96″/E 6°51′33.04″	<2	Cataclastic serpentinite	Antigorite + trem + talc + mgt
PSB12-6	N 45°41′42.90″/E 6°51′23.77″	<2	Massive serpentinite with preserved mesh textures	Antigorite + mgt
PSB12-11	N 45°42′32.17″/E 6°51′5.38″	10–15	Massive serpentinite with interlocking antigorite	Antigorite + trem + carb + talc + mgt
PSB12-17	N 45°41′43.55″/E 6°51′27.31″	~5	Blocky serpentinite between two faults	Antigorite + trem + talc + mgt
PSB12-Sample1	N 45°41′46.48″/E 6°51′36.54″	15–20	Statically serpentinized peridotite with preserved mantle foliation (cm scale)	Antigorite + mgt
PSB12-Sample2	N 45°41′39.55″/E 6°51′17.80″	<2	Foliated serpentinite	Antigorite + trem + talc + mgt
Chlorite schist				
PSB12-16	N 45°41′39.52″/E 6°51′19.83″	0	Chlorite schist	Chlorite + titanite
Continental Basement/Metasediments				
PSB12-12	N 45°42′39.16″/E 6°51′6.73″		Polymictic breccia in gray mica schist matrix	
PSB12-13	N 45°42′38.83″/E 6°51′6.69″		Cataclastic leucogranite	
PSB12-14	N 45°42′39.35″/E 6°51′6.68″		Gray mica schist	
PSB12-15	N 45°42′36.27″/E 6°51′9.75″		Meta-marl (calc-schist)	
St. Barthelemy				
Serpentinites				
SB12-1	N 45°47′31.28″/E 7°29′19.82″	<1	Serpentinite	Antigorite + mgt + carb
SB12-2	N 45°47′31.05″/E 7°29′19.59″	7	Massive serpentinite	Antigorite + mgt + carb
SB12-3	N 45°47′30.85″/E 7°29′18.90″	20	Massive serpentinite	Antigorite + mgt + carb vein
SB12-4	N 45°47′30.94″/E 7°29′17.93″	40	Massive serpentinite	Antigorite + mgt + carb
Metasediments				
SB12-5	N 45°47′31.52″/E 7°29′20.18″		Mica schist	
Rocca Canavese Zone (*Levone River sequence*)				
Serpentinites				
LV12-3	N 45°19′34.60″/E 7°35′50.78″	0	Omphacitite	Omphacite
LV12-4	N 45°19′35.39″/E 7°35′49.06″	30	Massive serpentinite	Antigorite + mgt + trem
LV12-5	N 45°19′34.60″/E 7°35′50.78″	<1	Massive serpentinite	Antigorite + mgt + trem
LV12-6	N 45°20′4.43″/E 7°35′2.31″	>150	Massive serpentinite with relict pyroxene	Antigorite + mgt + spinel + cpx + opx
Canavese Zone				
Serpentinites				
LV12-1	N 45°19′52.26″/E 7°36′22.13″	30–40	Massive serpentinite	Serpentine + mgt + carb + trem
LV12-2	N 45°19′52.07″/E 7°36′25.59″	1	Sheared serpentinite	Serpentine + mgt + trem

basement (Fig. 3M). It consists of serpentine and abundant fine-grained magnetite. It is overprinted by tremolite and highly cross-cut by carbonate veins (Fig. 3N). LV12-2 is a highly sheared serpentinite located 1 m from radiolarian chert (Fig. 3M) and consists of serpentine and magnetite (Fig. 3O). The serpentine mineral in samples LV12-1 and LV12-2 was difficult to determine by XRD and may represent mixed serpentine phases (Table 1).

4. Methods

4.1. Major and trace-element geochemistry

Samples were cut with a rock saw to remove weathering and obtain clean blocks for powdering. Samples were powdered in an alumina ceramic ball mill that is used solely for peridotite samples. Bulk major element analyses were determined by Actlabs (Ancaster, Ontario, Canada) using a lithium metaborate/tetraborate fusion method with subsequent analyses on an ICP-MS. A minimum detection limit of 0.01 wt.% for SiO_2, Al_2O_3, Fe_2O_3, MgO, CaO, Na_2O, K_2O, and P_2O_5 and 0.001 wt.% for MnO and TiO_2 is reported. Dissolutions for bulk trace element geochemistry were performed in the Radiogenic Isotope Clean Lab facility at the University of Texas at Austin and solutions were analyzed by ICP-MS at Rice University. Fifty to eighty milligrams of powdered sample, 250 μL of ultrapure HF, and 1 mL of ultrapure HNO_3 were loaded into 2.5 mL wrench-top Savillex beakers. Beakers were wrenched down, agitated in an ultrasonic bath for 20 min and heated in a gravity oven at 135 °C overnight. Samples were dried down on a hot plate and the HF/HNO_3 step was repeated. After samples were dried down again, 1 mL of HNO_3 was added. Samples were agitated for 30 min and heated in an oven at 150 °C for 3 h. Samples were dried down again and the HNO_3 step was repeated. The contents of the beakers were then diluted up in 125 g of 2% HNO_3 and spiked with Indium to achieve an internal standard at the level of 1 ppb. Samples were introduced into a magnetic sector ICP-MS (ThermoFinnigan Element 2) via solution using a 100 microliter/minute Elemental Scientific Teflon nebulizer coupled with a cyclonic spray chamber. Most of the trace elements were analyzed in low mass resolution mode ($m/\Delta m = 300$). The first series transition metals (V, Cr, Sc, Co, Mn, Fe, Cr, Ni) were analyzed in medium mass resolution mode ($m/\Delta m = 3000$) to avoid isobaric molecular interferences (oxides and argides). Sensitivity in low and medium mass resolution modes was 10^6 and 10^5 cps/pbb, respectively. USGS basalt standards BHVO-2 and BCR were used as external standards.

Major and minor element compositions of spinel and pyroxene grains were determined using the Cameca JEOL 8200 at the University of Texas at Austin. Single spots were analyzed using a 15 keV accelerating voltage, 10 nA beam current, and a beam size of 2 μm for pyroxenes and spinels. Probe standards used were natural Cr-augite (Si, Ca, Mg), ilmenite (Fe, Mn, Ti), Amelia albite (Na), chromite (Cr, Al) and synthetic Ni-olivine (Ni). A 30 s on peak count time was employed for all elements on WDS spectrometers. Chromite and Kakanui augite standards were analyzed as unknowns to ensure internal consistency. Trace element composition of relict pyroxenes was determined using LA-ICP-MS at the University of Texas at Austin using a New Wave UP193-fx (193 nm, 4–6 ns pulse width) excimer laser coupled to an Agilent 7500ce ICP-MS. Laser ablation parameters were optimized based upon tests of pyroxene unknowns. A large (150 μm) spot was selected to optimize sensitivity. Laser power, repetition rate, and He flow were iteratively modulated to obtain the most stable settings over 45-second dwell times. The best settings were determined to be 75% laser power, 10 Hz repetition rate, and a He flow of 250 mL/min. The 75% laser power setting corresponds to an average energy density (fluence) of ~9.79 ± 0.21 J/cm^2. Pulse-to-pulse laser power variation was maintained within 2.14% of this value during analysis. All samples were pre-ablated for 2 s using a 150 μm spot, 30% laser power, and 10 Hz repetition rate. The quadrupole method involved measurement of 25 analytes, using integration times between 10 and 300 ms. A gas blank interval of 40 s was used between all laser measurements to establish baseline sensitivities. Pyroxene analyses were bracketed hourly by triplicate analyses of laser ablation standards NIST-612, NIST-610, and USGS BCR-2G. Elemental concentrations were derived using Iolite software (Hellstrom et al., 2008), with ^{29}Si as the internal standard and NIST-612 as the primary calibration standard. Sample data were reduced based on the SiO_2 content in the pyroxenes obtained from EMPA analysis. Recoveries on BCR-2G and NIST-610 were within 1% and 7%, respectively, of GeoReM (http://georem.mpch-mainz.gwdg.de) preferred values.

4.2. Stable isotope geochemistry

Oxygen, hydrogen, and chlorine stable isotope ratios were measured at the University of Texas at Austin. Serpentinite samples were coarsely crushed and washed in dilute HCl overnight to remove any carbonate material. Serpentine grains were then hand-picked under a binocular microscope to ensure the visual absence of magnetite inclusions. ~2.0 mg of serpentine was measured using the laser fluorination method of Sharp (1990) to determine the $\delta^{18}O$ value. In order to check for precision and accuracy of oxygen analyses, garnet standard UWG-2 ($\delta^{18}O$ value = +5.8‰) (Valley et al., 1995), olivine standard San Carlos ($\delta^{18}O$ value = +5.2‰), and quartz standards Gee Whiz ($\delta^{18}O$ value = +12.6‰) and Lausanne-1 ($\delta^{18}O$ value = +18.1‰) were run. All $\delta^{18}O$ values are reported relative to SMOW, where the $\delta^{18}O$ value of NBS-28 is +9.65‰. Precision is ± 0.1‰.

δD values of bulk rock powders were determined on ~1 mg of material using the methods of Sharp et al. (2001). The error on each δD analysis is ±2‰. The sample powders were loaded into silver capsules, which are pyrolized in a ThermoElectron MAT TC-EA (high temperature conversion elemental analyzer). All samples were normalized to biotite standard NBS-30 (δD value = −65‰).

Chlorine stable isotope methods are based on the procedures of Eggenkamp (1994) and Magenheim et al. (1994) as modified by Barnes and Sharp (2006) and Sharp et al. (2007). Cl^- was released from bulk powdered samples to an aqueous solution by pyrohydrolysis (Magenheim et al., 1994). Cl^- was precipitated from solutions as AgCl via reaction with $AgNO_3$ (Eggenkamp, 1994). AgCl was filtered onto quartz filters and reacted with CH_3I to produce CH_3Cl, the analyte introduced into the mass spectrometer. CH_3Cl was purified of excess CH_3I on a dedicated gas chromatographic system in a continuous He flow prior introduction in the mass spectrometer. All $\delta^{37}Cl$ values are reported relative to SMOC (Standard Mean Ocean Chloride; $\delta^{37}Cl$ value = 0‰). Precision is ±0.2‰, based on three internal seawater standards and one internal serpentinite standard. All stable isotope analyses were made on a ThermoElectron MAT 253 mass spectrometer configured with an H/D collector and an additional collector/matched amplifier system specifically aligned for simultaneous measurement of masses 50 and 52.

5. Results

5.1. Bulk rock geochemistry

All serpentinite samples have high loss-on ignition (LOI) values (9.1 to 12.7 wt.%), consistent with petrographic observations of extensive serpentinization (Table 2). Antigorite contains stoichiometrically less water than lizardite (~12 wt.% H_2O compared to ~13 wt.% in lizardite) (e.g., Evans, 2004), accounting for the near 12 wt.% LOI in most of the samples. LOI values near 10 wt.% and lower are found only in three serpentinite samples (PSB12-1, PSB12-4, PSB-Sample2) and can be explained by the presence of talc, which is observed in thin section. This is also evident by the slightly lower MgO concentrations (30.0 to 31.3 wt.%; unnormalized) in these three samples (Table 2). MgO/SiO_2 and Al_2O_3/SiO_2 anhydrous wt.% ratios of the serpentinite samples range from 0.72 to 0.96 and 0.03 to 0.09, respectively (Fig. 4). These values are consistent with moderate amounts of melt depletion. Samples with low MgO/SiO_2 values (PSB12-1, PSB12-4, PSB-Sample2), below those of typical abyssal peridotites (field defined by Niu (2004)), are due to the presence of talc. Al_2O_3 and CaO concentrations range from 0.99 to 3.46 wt.% and 0.03 to 3.18 wt.%, respectively. High CaO concentrations (>1 wt.%) are due to the presence of tremolite. Cr and Ni concentrations range from 2083 to 4008 ppm and 1754 to 2887 ppm, respectively (Table 2). The bulk geochemistry of the chlorite schist reflects its monomineralic composition of chlorite. SiO_2 concentrations in chlorite schist are low; whereas, MgO, Al_2O_3, total Fe, and water contents (based on LOI) are high (Table 2).

Bulk serpentinite samples have high incompatible trace element and rare earth element (REE) concentrations compared to typical mid-ocean ridge serpentinites (Fig. 5A and B) (e.g., Kodolányi et al., 2012). REE patterns are slightly depleted in LREE (La_N/Sm_N = 0.17–1.89; La_N/Yb_N = 0.12–2.36; Sm_N/Yb_N = 0.41–3.18; $_N$ = C1-chondrite normalized (McDonough and Sun, 1995)) (Fig. 5A). Trace element patterns normalized to primitive mantle show large enrichments in Cs, U, and Pb (Fig. 5C).

5.2. Pyroxene and spinel geochemistry

Relict pyroxene (both clinopyroxene and orthopyroxene) and spinel were only identified in sample LV12-6. Clinopyroxenes and orthopyroxenes have an average Mg# value of 0.917 and 0.903, respectively (Table 3). Clinopyroxenes have average Al_2O_3, Cr_2O_3, and TiO_2 concentrations of 6.50 wt.%, 0.79 wt.%, and 0.46 wt.%, respectively (Table 3, Fig. 6). Primitive mantle-normalized trace element patterns for clinopyroxenes show highly variable LREE concentrations, with some grains depleted and others enriched in LREE relative to MREE and HREE concentrations. Zr is highly depleted in all grains (Fig. 7). As expected, orthopyroxene has overall lower REE concentrations than clinopyroxene. LREE concentrations are also highly variable, but tend to be lower than MREE and HREE concentrations (Fig. 7). Spinels have Mg# values of 0.792–0.803 and Cr# values of 0.078–0.094 (Table 4, Fig. 8).

5.3. Stable isotope geochemistry

$\delta^{18}O$ and δD values of the serpentinites range from +5.2 to +9.4‰ and −101 to −52‰, respectively (Table 5, Fig. 9). $\delta^{37}Cl$ values of the serpentinites range +0.5 to +2.4‰. These are some of the highest

Table 2
Major and trace element composition of serpentinite and chloritite samples.

	PSB12-1	PSB12-4	PSB12-6	PSB12-11	PSB12-16	PSB12-17	PSB-Sample 1	PSB-Sample 2	LV12-1	LV12-2	LV12-4	LV12-5	SB12-1	SB12-2	SB12-3	BHVO-2	BCR
	serp	serp	serp	serp	chloritite	serp	serp	serp	serp	serp	serp	serp	serp	serp	serp		
Major elements (wt.%)																	
SiO_2	41.89	42.38	40.99	40.21	31.37	41.90	39.59	42.37	39.06	39.68	40.38	40.17	42.50	39.06	41.38		
Al_2O_3	2.24	2.87	2.43	2.80	17.30	2.10	3.30	2.61	3.24	2.59	3.46	3.29	1.36	0.99	1.47		
Fe_2O_3(T)	15.33	8.38	8.09	8.72	15.21	8.29	7.93	10.07	8.84	8.26	7.91	7.33	6.42	7.99	6.23		
MnO	0.058	0.130	0.168	0.160	0.192	0.178	0.156	0.177	0.129	0.106	0.116	0.107	0.067	0.065	0.098		
MgO	29.96	31.32	35.28	35.26	21.51	34.11	35.40	30.62	32.89	34.48	33.27	35.13	36.31	37.55	38.02		
CaO	0.20	2.53	0.04	0.54	1.36	1.21	0.07	3.15	1.89	1.06	3.18	1.50	0.04	0.03	0.12		
Na_2O	0.02	0.04	0.01	0.01	0.01	0.02	0.02	0.03	0.12	0.02	0.08	0.02	0.02	0.02	0.01		
K_2O	0.02	0.02	0.01	<0.01	<0.01	<0.01	0.01	0.01	0.01	<0.01	0.01	0.01	0.01	<0.01	<0.01		
TiO_2	0.085	0.076	0.045	0.085	1.539	0.081	0.102	0.087	0.13	0.068	0.098	0.07	0.032	0.017	0.033		
P_2O_5	0.02	0.03	0.02	0.02	0.47	0.03	0.02	<0.01	0.02	0.03	0.02	0.02	0.01	0.02	0.02		
LOI	9.07	10.14	12.12	11.80	10.25	11.09	11.96	9.70	11.89	12.7	10.75	11.66	11.88	12.3	11.95		
Total	98.88	97.91	99.21	99.61	99.21	99.01	98.56	98.85	98.23	99.01	99.27	99.31	98.66	98.04	99.34		
Mg#	0.777	0.869	0.886	0.878	0.716	0.880	0.888	0.844	0.869	0.882	0.882	0.895	0.910	0.893	0.916		
Trace elements (ppm)																	
Be	1.18	0.239	0.2450	0.09585	0.818	0.0465	0.1400	0.252	0.0179	0.01375	0.01495	0.0253	0.05955	0.0565	0.03095	1.00	2.25
Sc	12.1	14.7	10.7	14.8	22.4	19	12.8	14.1	15.5	14	16.2	12	8.13	8.71	7.87	33.3	31.9
V	71.8	85.9	55.6	75.6	162	64.7	66.2	75.8	80.0	67.1	79.1	55.8	31.1	33	31.9	294	432
Cr	3122	2729	2275	3714	416	4008	2381	3062	2228	2083	2678	2789	2488	2773	2564	280	14.8
Co	142	110	88.4	87.9	44.2	114	81.5	136	116	107	86.5	111	104	108	105	43.2	39
Ni	2887	2420	2260	1799	610	2611	2104	2587	1895	2038	1780	2269	2133	2782	1754	120	12.4
Cu	2.94	24.0	76.4	15.1	0.175	48.7	2.95	6.41	22.8	7.02	42.2	3.71	6.56	12.2	17.5	128	18.2
Zn	128	158	116	127	205	309	113	223	146	112	41.7	37.8	40.7	30.2	47.9	111	121
Sr	3.85	2.61	1.27	12.1	13	5.85	0.721	12.3	6.68	8.7	9.96	3.54	1.38	0.559	1.41	392	344
Y	1.26	2.19	2.71	1.40	41.3	1.43	1.42	2.41	3.80	2.38	2.90	2.05	0.378	0.522	0.700	27.1	36.3
Zr	1.02	1.57	1.88	0.994	3.6	1.22	0.871	1.27	4.84	1.55	1.94	2.71	0.949	0.969	1.07	166	190
Nb	0.262	0.0358	0.0338	0.0343	16.7	0.0421	0.0338	0.0602	0.111	0.0343	0.0339	0.396	0.133	0.0676	0.270		
Cs	0.719	0.867	0.620	0.555	0.0347	0.623	0.255	0.85	0.789	0.442	0.0483	0.0524	0.409	0.0336	0.0398	0.0926	1.1
Rb	0.262	0.214	0.114	0.122	0.0537	0.127	0.0999	0.234	0.356	0.168	0.246	0.285	0.491	0.0566	0.0676	9.76	46.8
Ba	1.03	3.47	1.30	0.573	1.18	2.8	1.25	3.47	7.74	54.9	1.16	3.73	0.35	0.250	10.8	128	678
La	0.0480	0.149	0.153	BDL	1.89	BDL	0.0690	0.0807	0.109	0.0419	BDL	0.474	0.0407	0.0674	0.113	14.8	25.2
Ce	0.110	0.293	0.347	0.0206	10.7	0.026	0.14	0.143	0.463	0.0737	0.0529	0.952	0.0506	0.15	0.314	36.7	53.5
Pr	0.018	0.0476	0.0510	0.00785	2.24	0.0166	0.0237	0.0292	0.0973	0.0285	0.0246	0.112	0.0089	0.0245	0.0621	5.24	6.78
Nd	0.111	0.303	0.319	0.0955	13.4	0.169	0.14	0.215	0.608	0.249	0.239	0.486	0.0521	0.134	0.303	24.2	29.0
Sm	0.0613	0.155	0.157	0.0761	5.42	0.123	0.0695	0.132	0.275	0.15	0.160	0.157	0.0236	0.0525	0.0947	6.07	6.59
Eu	0.0290	0.0706	0.0537	0.0191	1.49	0.0637	0.0213	0.0432	0.107	0.0760	0.0682	0.0397	0.0067	0.0188	0.0373	1.95	2.08
Tb	0.0176	0.0368	0.0395	0.0200	0.928	0.0283	0.0194	0.0359	0.0610	0.0351	0.0405	0.0337	0.00535	0.0101	0.0139	0.930	1.06
Dy	0.191	0.367	0.412	0.225	7.69	0.272	0.214	0.373	0.599	0.369	0.439	0.303	0.0549	0.0861	0.0881	5.28	6.44
Ho	0.0441	0.0778	0.0926	0.0514	1.50	0.0562	0.0496	0.0834	0.133	0.0825	0.0999	0.0686	0.0131	0.0182	0.0157	0.970	1.29
Er	0.118	0.189	0.238	0.129	3.63	0.135	0.132	0.213	0.334	0.207	0.254	0.183	0.0361	0.0462	0.0397	2.60	3.63
Tm	0.0257	0.0363	0.0468	0.0260	0.592	0.025	0.0271	0.0414	0.0625	0.040	0.0500	0.0339	0.0082	0.0088	0.00545	0.336	0.537
Yb	0.161	0.215	0.279	0.156	3.44	0.15	0.161	0.249	0.367	0.237	0.3	0.21	0.0494	0.0553	0.0324	2.12	3.32
Lu	0.0269	0.0330	0.0441	0.0266	0.447	0.0233	0.026	0.0402	0.0584	0.0386	0.0499	0.0359	0.00845	0.009	0.0041	0.291	0.495
Hf	0.0674	0.0942	0.0707	0.0764	0.24	0.0717	0.0620	0.0754	0.178	0.0827	0.104	0.0936	0.0375	0.0281	0.0426	4.29	4.95
Ta	0.0056	0.0016	0.002	0.0016	0.8605	0.0019	0.00135	0.0011	0.0043	0.00175	0.00135	0.00855	0.0053	0.0038	0.0153		
Tl	0.0069	0.0135	0.0148	0.0094	BDL	0.0479	0.0043	0.0171	0.0337	0.01620	BDL	0.0048	0.0247	0.0063	0.0023	0.015	0.257
Pb	22.8	18.0	43.3	0.688	3.67	10.2	1.23	6.28	2.82	0.813	0.198	0.56	0.513	2.59	0.236	1.73	11
Th	0.008	0.00585	0.0051	0.0025	0.180	0.0033	0.00595	0.0027	0.017	0.00420	0.0022	0.0093	0.0106	0.0063	0.0412	1.19	5.71
U	0.972	1.16	0.0661	0.0685	0.314	0.125	0.0574	0.965	0.00595	0.00270	0.00405	0.0176	0.159	0.0111	0.0563	0.403	1.69

BDL = below detection limits.

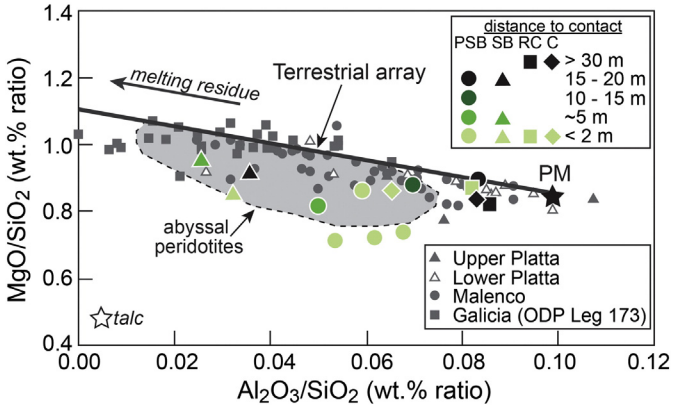

Fig. 4. Bulk rock major element ratios of Al_2O_3/SiO_2 (anhydrous) vs. MgO/SiO_2 (anhydrous) of Punta Rossa (PSB; circles), St. Barthelemy (SB; triangles), Rocca Canavese (RC; squares), and Canavese (C; diamonds) serpentinites. Sample data is color coded to indicate distance from contact with sedimentary unit and/or continental basement. PM (star) = primitive mantle from McDonough and Sun (1995). The black line is the "terrestrial array" (Jagoutz et al., 1979) in which partial melt extraction (indicated by the black arrow) will leave the residue with higher MgO/SiO_2 and lower Al_2O_3/SiO_2 than the melt. The gray area highlights a global compositional range of abyssal peridotites (Niu, 2004). Also shown for comparison are peridotites from the Platta (triangles) and Malenco (small gray circles) (Müntener et al., 2010) and from the Galicia Margin (Leg 173) (squares) (Hébert et al., 2001). The geochemistry of the serpentinites is partially controlled by the degree of melt extraction from the original peridotite, but also deviates from this trend due to modal mineralogy (e.g., presence of talc). (For interpretation of the references to color in this figure legend, the reader is referred to the web version of this article.)

$\delta^{37}Cl$ values reported for serpentinites to date. Most seafloor serpentinites have values ranging from −2 to +0.5‰, with rare seafloor serpentinites having $\delta^{37}Cl$ values ≥+1.0‰ (Barnes and Sharp, 2006; Barnes et al., 2008, 2009; Bonifacie et al., 2008; Boschi et al., 2013). A few obducted serpentinites and meta-peridotites have values as high as +1.7‰ (Barnes et al., 2006, 2013; John et al., 2011) and +2.1‰ (Selverstone and Sharp, 2011), respectively. $\delta^{37}Cl$ values of the continental basement and metasediments are heterogeneous, ranging from −1.2 to +1.3‰; whereas, δD values are relatively homogeneous ranging from −54 to −47‰ (Table 5). These $\delta^{37}Cl$ values are consistent with published $\delta^{37}Cl$ values of HP and UHP metasediments (−3.7 to +2.2‰ with the majority having negative values) (John et al., 2010; Selverstone and Sharp, 2013). The chlorite schist has $\delta^{18}O$, δD, and $\delta^{37}Cl$ values of +7.4‰, −50‰, and +1.5‰, respectively (Table 5).

6. Discussion

6.1. Tectonic provenance of the serpentinite protolith

The geochemical data presented above can be used to place constraints on the origin of the studied serpentinites and on the tectonic setting of their serpentinization.

6.1.1. Trace element data

Spinels from LV12-6 (only sample preserving relict spinel) have extremely low Cr#s (average = 0.087) and high Mg#s (average = 0.798) suggesting very low degrees of melt depletion, less than observed at the Iberia and Newfoundland margins (Fig. 8). The spinel compositions are similar to spinels from Malenco, Totalp, and Upper Platta peridotites (Müntener et al., 2010) (Fig. 8), all of which are interpreted as peridotites exhumed near the continental margin (e.g., Manatschal and Müntener, 2009). Clinopyroxenes have high Al_2O_3, Cr_2O_3, and TiO_2 concentrations (average = 6.50 wt.%, 0.79 wt.%, and 0.46 wt.%, respectively) also placing them within the compositional field of abyssal peridotites (Table 3, Fig. 6).

The overall high bulk concentrations in REE and slightly depleted LREE concentrations in serpentinites from all localities in this study are consistent with smaller degrees of melt extraction as is expected for abyssal serpentinites compared to serpentinites from the fore-arc mantle wedge. A geochemical compilation by Kodolányi et al. (2012) indicates that serpentinites from passive margin settings have overall higher REE concentrations than those from mid-ocean ridges, suggesting that the studied REE-enriched serpentinites are consistent with derivation from a passive margin setting. These REE patterns are identical to those observed from the Galicia and Newfoundland margins (Kodolányi et al., 2012) (Fig. 5A and B), as well as, serpentinites from Platta and Malenco in the Eastern Alps, which originated from an ocean–continent transition (Fig. 5B) (Müntener et al., 2010). However, there is large variability in REE concentrations in abyssal serpentinites, thus making a conclusion based solely on trace element geochemistry tenuous (Deschamps et al., 2013). The high bulk REE concentrations, particularly high LREE concentrations, may also be due to some refertilization by melts prior to serpentinization (Niu, 2004; Paulick et al., 2006; Kodolányi et al., 2012; Deschamps et al., 2013). This feature, which has been widely documented in the better-preserved Tethyan mantle peridotites (e.g., Müntener and Piccardo, 2003; Müntener et al., 2010; Piccardo, 2010), would still be consistent with an origin from sub-continental mantle. Furthermore, the possibility that the observed high REE concentrations might be related to the presence of talc (Paulick et al., 2006; Deschamps et al., 2013) can be discounted for this study, as all serpentinites have high REE concentrations regardless of the presence or absence of talc. Relict clinopyroxenes from sample LV12-6 show similar overall high REE concentrations, as in the bulk rock (Fig. 7), with some clinopyroxene grains having notably high LREE concentrations.

In addition, the overall concentration of bulk trace elements, even for samples that experienced only limited subduction-related interaction with crustal rocks (see below), is high, also consistent with smaller degrees of partial melting and/or refertilization by metasomatising melts. Cs, U, and Pb are particularly high in concentration (>10 to >100 times that of primitive mantle concentrations). Cs, U, and Pb are enriched in abyssal serpentinites, including those that have undergone subduction and exhumation (Kodolányi et al., 2012; Deschamps et al., 2013). Sr concentrations are similar to those observed in serpentinites from the Galicia and Newfoundland margins and not as high as Sr concentrations in mantle wedge or carbonate-rich mid-ocean ridge serpentinites (Kodolányi et al., 2012).

Therefore, we conclude that the overall high REE and trace concentrations and flat REE patterns are consistent with the structural and lithostratigraphic interpretation of the Punta Rossa unit, Canavese, and St. Barthelemy areas as a hyper-extended lithospheric margin. REE and trace element data of serpentinized peridotites from the Rocca Canavese Zone also suggest an origin from a hyper-extended lithospheric margin.

6.1.2. Stable isotope data

The final stable isotopic (O, H, Cl) composition of serpentinite will be determined by the isotopic composition of the serpentinizing fluid, the temperature of serpentinization, the fluid/rock ratios of serpentinization, and post-serpentinite fluid interaction. This information can be used to place constraints on the tectonic setting of serpentinization (e.g., Burkhard and O'Neil, 1988; Früh-Green et al., 1990, 1996, 2001; Sakai et al., 1990; Yui et al., 1990; Cartwright and Barnicoat, 1999; Kyser et al., 1999; Skelton and Valley, 2000; Alt and Shanks, 2006; Barnes and Sharp, 2006). Peridotite that has not interacted with external fluids should have a bulk $\delta^{18}O$ value of ~5.5‰ (Mattey et al., 1994). The dashed gray line in Fig. 9 shows the calculated $\delta^{18}O$ and δD values of serpentine in equilibrium with seawater at a given temperature (Saccocia et al., 2009). $\delta^{18}O$ values of serpentinites from

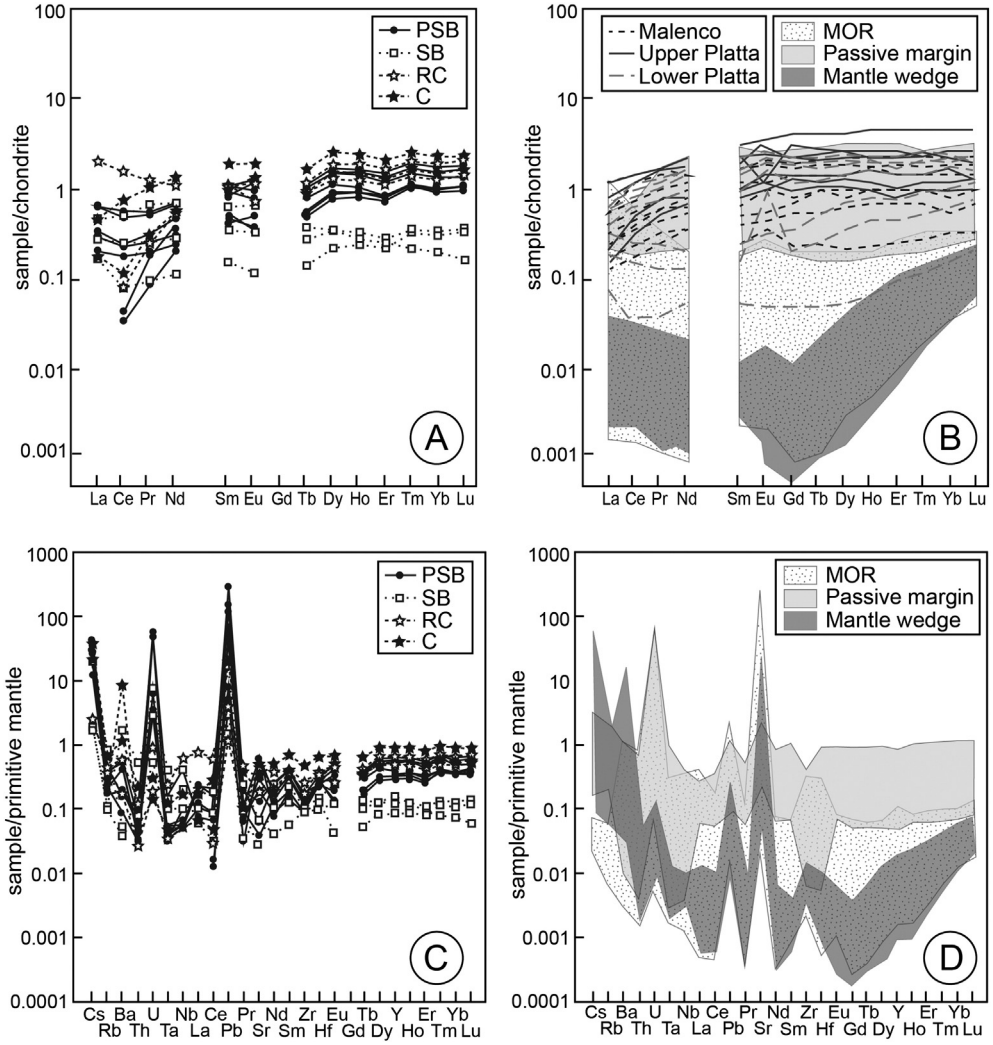

Fig. 5. Bulk serpentinite REE and trace element data. A) Chondrite normalized REE compositions of Punta Rossa (PSB; circles), St. Barthelemy (SB; squares), Rocca Canavese (RC; open stars), and Canavese (C; solid stars) serpentinites. Chondrite normalizing values from McDonough and Sun (1995). B) Range of chondrite normalized REE concentrations of ODP serpentinized peridotites from three different tectonic settings: mid-ocean ridge (MOR; Mid-Atlantic Ridge (Leg 209) and Hess Deep (Leg 147)), passive margin (Iberia Abyssal Plain (Leg 173) and Newfoundland (Leg 210), and mantle wedge (Guatemala (Leg 84) and Mariana (Leg 195) (Kodolányi et al., 2012). Chondrite normalized REE concentrations of serpentinized peridotites from the Platta and Malenco units are shown for comparison (Müntener et al., 2010). C) Primitive mantle normalized trace element compositions of Punta Rossa (PSB; circles), St. Barthelemy (SB; squares), Rocca Canavese (RC; open stars), and Canavese (C; solid stars) serpentinites. Primitive mantle normalizing values from McDonough and Sun (1995). D) Range of primitive mantle normalized trace concentrations of ODP serpentinized peridotites from three different tectonic settings (same settings as in B) (Kodolányi et al., 2012).

this study are consistent with serpentinization temperatures between 150 and 200 °C by seawater on the seafloor. These oxygen isotope data are consistent with the predominantly high $\delta^{18}O$ values of serpentinites from the Galicia Margin (8.9 to 11.7‰ from Leg 103, Hole 637A (Agrinier et al., 1988); 8.8 to 12.2‰ from Leg 149, Holes 897C and 897D (Agrinier et al., 1996); 6.5 to 8.6‰ from Leg 173, Hole 1068A and 3.9 to 7.3‰ from Leg 173, Hole 1070A (Skelton and Valley, 2000)), suggesting low temperatures of serpentinization (<200 °C) by seawater.

6.2. Interaction with sedimentary-derived fluids during Alpine subduction and exhumation

Bulk REE and trace element data indicate protolith derivation from an abyssal setting, likely a hyper-extended lithospheric margin. Based on oxygen isotope data, it is likely that the bulk of serpentinization occurred at or near the seafloor. As shown below, trace element and stable isotope compositional transects with decreasing distance to the sediment/serpentinite interface, particularly in the well-exposed Punta Rossa unit, also support subsequent interaction with metasedimentary derived fluids during Alpine subduction and/or exhumation.

6.2.1. Stable isotope data

In contrast to the oxygen isotope data, which supports low-temperature interaction with seawater, the hydrogen and chlorine isotope data are more ambiguous. All serpentinite δD values (−101 to −52‰) from this study are lower than predicted by equilibration with seawater (Fig. 9). Low δD values are common in terrestrial serpentinites and are generally thought to be due to post-serpentinization and post-emplacement interaction with meteoric water at low temperature (Kyser and Kerrich, 1991; O'Hanley, 1996). However, antigorite is harder to reset by post-serpentinization interaction with meteoric water compared to lizardite and chrysotile (Kyser et al., 1999). Because the serpentinites from this study consist predominantly of antigorite, post-

Table 3
Major and trace element concentrations in relict pyroxenes in sample LV12-6.

Major elements (wt.%)

	CPX	CPX	CPX	CPX	CPX	CPX	CPX	CPX	CPX	OPX	OPX	OPX	OPX	OPX	OPX	OPX
SiO_2	51.28	51.47	51.91	51.65	51.72	51.30	51.42	51.26	51.17	54.97	54.30	54.64	54.28	54.69	54.18	54.17
TiO_2	0.42	0.48	0.43	0.46	0.48	0.48	0.46	0.48	0.45	0.07	0.09	0.10	0.08	0.13	0.15	0.11
Al_2O_3	6.93	6.86	6.36	6.39	6.41	5.94	6.56	6.43	6.67	3.78	2.95	3.64	3.94	4.36	4.78	4.96
FeO	2.44	2.34	2.45	2.35	2.49	2.55	2.38	2.27	2.29	6.51	5.12	6.65	6.67	6.60	6.37	6.35
MnO	0.08	0.10	0.08	0.07	0.10	0.10	0.09	0.08	0.08	0.15	0.14	0.15	0.14	0.15	0.15	0.14
MgO	14.42	14.53	14.72	14.73	15.37	15.29	14.68	14.66	14.35	33.88	29.97	34.33	34.04	33.92	32.89	32.97
CaO	21.58	21.84	21.87	21.91	21.03	21.68	21.78	21.53	21.47	0.39	6.21	0.32	0.49	0.42	1.40	0.82
Na_2O	1.63	1.70	1.59	1.57	1.52	1.47	1.55	1.58	1.72	0.01	0.06	0.02	0.04	0.03	0.10	0.07
Cr_2O_3	0.83	0.80	0.77	0.78	0.79	0.74	0.73	0.79	0.83	0.30	0.25	0.26	0.32	0.35	0.40	0.39
NiO	0.03	0.06	0.04	0.01	0.03	0.03	0.04	0.07	0.04	0.10	0.05	0.08	0.06	0.08	0.08	0.07
Total	99.65	100.18	100.21	99.94	99.94	99.56	99.70	99.13	99.06	100.15	99.13	100.19	100.07	100.73	100.51	100.05
Mg#	0.913	0.917	0.915	0.918	0.917	0.915	0.916	0.920	0.918	0.903	0.913	0.902	0.901	0.902	0.902	0.903

Trace elements (ppm)

	CPX	CPX	CPX	CPX	CPX	CPX	CPX	CPX	CPX	OPX	OPX	OPX	OPX	OPX	OPX	OPX	OPX
Rb	2.14	bdl	0.61	0.05	0.31	0.13	0.56	0.11	0.16	1.08	0.28	0.31	0.21	0.16	0.76	0.10	0.76
Th	0.66	bdl	0.07	0.01	0.00	0.06	0.07	0.02	0.03	0.01	0.01	0.01	bdl	bdl	0.00	0.00	0.01
U	0.59	bdl	0.06	0.00	bdl	0.00	0.02	0.00	0.01	0.01	0.01	0.01	bdl	0.00	0.01	0.00	bdl
Nb	1.31	bdl	0.15	0.01	0.02	0.02	0.05	0.01	0.01	0.02	0.03	0.02	bdl	0.01	bdl	bdl	0.01
Ta	0.55	bdl	0.06	bdl	bdl	bdl	0.01	0.00	bdl	0.01	0.01	0.01	bdl	0.00	bdl	0.00	0.00
La	1.76	bdl	0.21	0.03	0.04	9.00	0.07	0.12	0.03	0.08	0.08	0.11	bdl	0.02	0.03	0.00	0.02
Ce	1.99	bdl	0.58	0.35	0.45	0.50	0.40	0.31	0.46	0.20	0.15	0.04	bdl	0.02	0.09	0.01	0.02
Pb	1.08	bdl	0.28	0.02	0.06	0.06	0.13	0.07	0.06	0.32	0.09	0.04	bdl	0.06	0.17	bdl	0.07
Sr	16.77	3.90	7.53	6.40	7.13	7.70	5.84	5.70	7.36	1.34	2.05	3.66	3.40	1.18	3.18	0.82	8.40
Nd	2.56	1.66	2.09	1.56	1.88	2.09	1.52	1.70	2.09	0.08	0.10	0.09	bdl	0.02	0.04	0.05	0.04
Sm	2.30	1.52	1.88	1.42	1.33	1.48	1.10	1.20	1.50	0.06	0.03	0.09	bdl	0.03	0.03	0.03	0.03
Zr	12.16	5.36	7.80	9.90	8.30	10.10	7.10	6.30	8.40	2.90	0.45	0.27	0.17	0.58	1.20	0.58	0.69
Hf	1.05	0.33	0.55	0.45	0.52	0.62	0.42	0.50	0.58	0.16	0.03	0.02	0.01	0.04	0.06	0.04	0.05
Eu	1.19	0.56	0.77	0.58	0.64	0.73	0.46	0.53	0.63	0.03	0.04	0.05	bdl	0.01	0.04	0.02	0.07
Ti	295.2	424.0	400.0	747.0	911.0	1530.0	1060.0	2201.0	2770.0	1160.0	390.0	179.0	93.8	105.8	107.5	137.9	150.0
Gd	2.50	2.34	2.28	1.98	2.06	2.73	1.77	1.78	2.14	0.12	0.04	0.12	bdl	0.03	0.05	0.06	0.05
Dy	3.44	3.22	3.57	3.11	2.99	3.66	2.78	2.52	3.57	0.20	0.10	0.21	0.08	0.10	0.11	0.17	0.19
Y	22.90	27.00	25.20	21.00	23.90	26.50	18.40	16.10	20.30	1.61	0.76	1.84	0.96	0.97	1.18	1.47	1.55
Er	2.45	2.03	2.25	1.86	2.04	2.30	1.84	1.93	2.28	0.18	0.10	0.18	0.13	0.13	0.15	0.17	0.17
Yb	2.30	1.91	2.16	1.67	2.03	2.38	1.71	1.82	2.16	0.17	0.24	0.26	0.25	0.21	0.28	0.24	0.31
Lu	0.73	0.11	0.33	0.24	0.29	0.35	0.27	0.28	0.31	0.03	0.05	0.05	bdl	0.04	0.05	0.05	0.05
V	162.8	220.0	191.0	261.0	321.0	314.0	259.0	275.0	312.0	242.0	98.8	91.0	78.2	81.9	88.5	95.9	95.6

emplacement resetting of δD values by meteoric water is likely minimal. Other researchers have suggested that low δD values reflect a component of magmatic or metamorphic fluid in the serpentinizing fluid (e.g., Burkhard and O'Neil, 1988; Früh-Green et al., 1996, 2001; Pelletier et al., 2008). For example, Früh-Green et al. (2001) argue that low δD values (−102 to −77‰) in Erro-Tobbio serpentinites reflect interaction with metamorphic fluids during the early stages of subduction. Pelletier et al. (2008) also conclude that low δD values of Alpine serpentinites in contact with crustal rocks are due to interaction with crustal derived fluids (see below for more discussion). Interestingly, δD values are remarkably low (−85 to −70‰; n = 4) for bulk serpentinites from the Galicia Margin (Leg 103, Hole 637A) (Agrinier et al., 1988). An explanation for these low δD values is not given, but it is postulated that magmatic or metamorphic fluids may have played a role (Agrinier et al., 1988). It is highly likely that the low δD values reported here are due to interaction with crustal-derived metamorphic fluids during Alpine metamorphism.

Chlorine stable isotopes have also recently been employed as a tracer of fluid source and hence, tectonic setting of serpentinization (e.g., Barnes and Sharp, 2006; Barnes et al., 2006; Selverstone and Sharp, 2011, 2013). Seafloor serpentinites formed by interaction with seawater typically have $\delta^{37}Cl$ values ranging from +0.2 to +0.5‰, whereas serpentinites that interacted with sedimentary pore fluids and/or sediment-derived fluid have $\delta^{37}Cl$ values of −2.0 to −0.5‰ (Barnes and Sharp, 2006). Seafloor serpentinites with the lowest measured $\delta^{37}Cl$ values (−2.0 to +0.1‰, average = −1.0 ± 0.5‰; n = 21) are from the Galicia Margin (ODP Leg 173 Hole 1068A). At this locality, serpentinites are overlain by 42 m of sedimentary breccia capped by 139 m of sediments and are interpreted as part of an ocean–continent transition (Shipboard Scientific Party, 1998a,b). Only few serpentinites with $\delta^{37}Cl$ values > +1.0‰, similar to those found in this study, have been documented and are typically observed in obducted high-pressure serpentinites (Barnes et al., 2006, 2008, 2013; John et al., 2011; Selverstone and Sharp, 2011). The origin of the of the high $\delta^{37}Cl$ values is unclear, particularly because it is unknown how the Cl isotope composition of oceanic and continental crust may be modified during subduction metamorphism. However, it has been postulated that serpentinites with high $\delta^{37}Cl$ values reflect interaction with fluid sourced from high-P metasediments or altered oceanic crust (John et al., 2010; Selverstone and Sharp, 2011; Barnes et al., 2013).

The $\delta^{18}O$, δD, and $\delta^{37}Cl$ values of the Punta Rossa serpentinites all show weak trends with distance to the contact with the metasedimentary breccia and continental basement. $\delta^{18}O$ values increase and δD and $\delta^{37}Cl$ values decrease with decreasing distance to the contact (Fig. 10). Sedimentary-derived fluids typically have high $\delta^{18}O$ values (~+10 to +30‰) (Sharp, 2007 and references therein). $\delta^{37}Cl$ values of the sedimentary and continental basement lithologies range from −1.2 to +1.3‰ (Table 5), equal to or lower than (within error) the $\delta^{37}Cl$ values of the serpentinites. The increasing $\delta^{18}O$ values and the decreasing $\delta^{37}Cl$

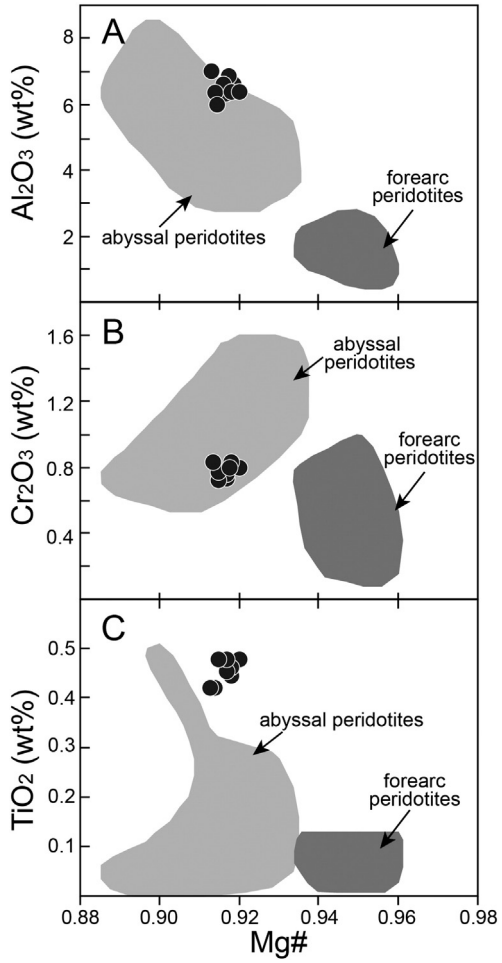

Fig. 6. Minor element compositional plots of clinopyroxene from sample LV12-6 (Rocca Canvese Zone). A. Mg# vs. Al_2O_3 (wt.%) B. Mg# vs. Cr_2O_3 (wt.%) C. Mg# vs. TiO_2 (wt.%). Compositional fields for abyssal peridotites defined by data from Johnson et al. (1990) and Hellebrand et al. (2002) and forearc peridotites defined by data from Parkinson and Pearce (1998) and Ishii et al. (1992).

values can all be explained by a fluid derived from the metasediments interacting with the serpentinites, possibly incorporated into antigorite during the transformation of lizardite to antigorite during subduction.

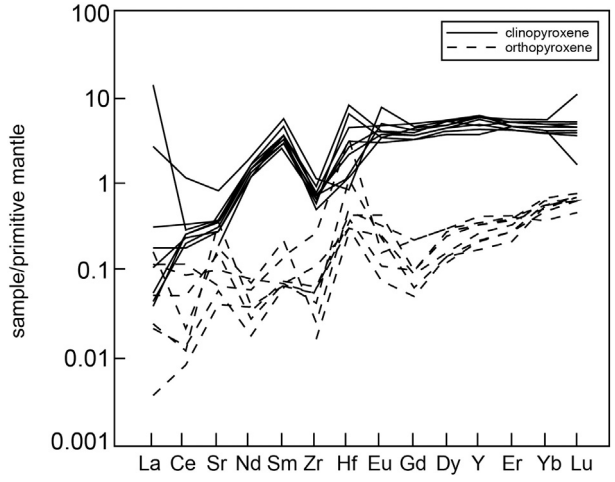

Fig. 7. Primitive mantle normalized REE and trace element compositions of clinopyroxene and orthopyroxene from sample LV12-6 (Rocca Canvese Zone). Primitive mantle normalizing values from McDonough and Sun (1995).

Table 4
Spinel composition from LV12-6.

	S1 (n = 5)	S2a (n = 3)	S2b (n = 3)	S4 (n = 3)	S5 (n = 4)	S6 (n = 4)
SiO_2	0.00	0.00	0.01	0.02	0.01	0.01
TiO_2	0.07	0.04	0.08	0.05	0.07	0.03
Al_2O_3	59.96	58.00	58.20	58.29	58.59	60.18
Cr_2O_3	7.69	8.94	8.75	8.49	8.77	7.58
Fe_2O_3	2.40	2.44	2.56	2.68	2.72	2.52
FeO	9.24	9.51	9.12	9.40	9.71	9.40
NiO	0.42	0.40	0.36	0.39	0.40	0.39
MnO	0.11	0.10	0.11	0.10	0.12	0.10
MgO	21.17	20.56	20.89	20.72	20.74	21.15
CaO	0.00	0.00	0.02	0.02	0.01	0.01
Na_2O	0.01	0.00	0.02	0.00	0.00	0.00
Total	100.81	99.71	99.85	99.86	100.87	101.08
Mg#	0.803	0.794	0.803	0.797	0.792	0.800
Cr#	0.079	0.094	0.092	0.089	0.091	0.078

FeO and Fe_2O_3 in spinel were calculated from stoichiometry.
Mg# = $Mg/(Mg + Fe^{2+})$.
Cr# = $Cr/(Cr + Al)$.

The highest $\delta^{18}O$ and lowest $\delta^{37}Cl$ values occur near the contact where the highest fluid/rock ratio was likely present. The Punta Rossa serpentinites show a decrease in δD values close to the contact. Similar to this study, Pelletier et al. (2008) also conducted a sampling transect across a serpentinite body in contact with crustal basement (Geisspfad serpentinite; Swiss-Italian Alps). They too note a decrease in the bulk δD values of the serpentinite near the contact with the gneiss. The serpentinite transitions from δD values of −30 to −56‰ (one outlier at −89‰) to values of −61 to −112‰ in the ophicarbonate nearest the contact. δD values were not determined for the metasomatic "blackwall" zone or the adjacent gneiss. These low δD values at the serpentinite rim were interpreted as interaction with crustal derived fluids (Pelletier

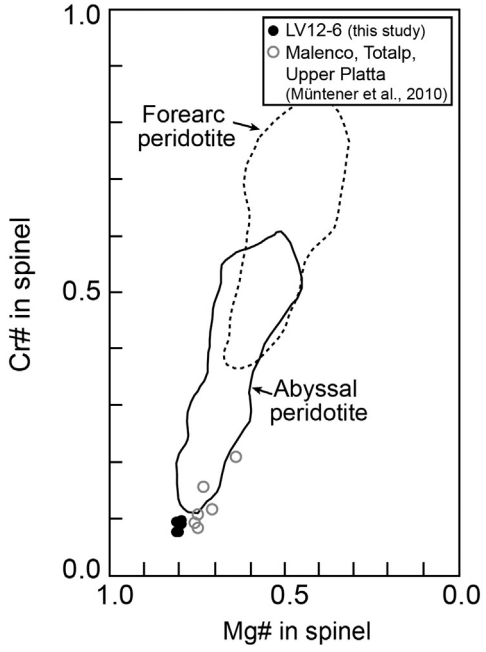

Fig. 8. Mg# (Mg/(Mg + Fe^{2+})) vs. Cr# (Cr/(Cr + Al)) for relict spinel from LV12-6 (Rocca Canavese Zone). The compositional fields for abyssal and forearc peridotites are from Tamura and Arai (2006) and references therein.

Table 5
Stable isotope compositions of the Punta Rossa unit.

Sample	$\delta^{18}O_{serp}$ (‰)	$\delta^{18}O_{chl}$ (‰)	$\delta^{18}O_{omp}$ (‰)	δD_{bulk} (‰)	$\delta^{37}Cl_{bulk}$ (‰)
Petite St. Bernard Pass (*Punta Rossa unit*)					
Serpentinites					
PSB12-1	8.2			−72, −73[a]	1.5
PSB12-4	8.2			−69, −67	1.3
PSB12-6	7.0			−72, −71	1.9
PSB12-11	6.9			−57, −58	1.9
PBS12-17	7.8			−58, −58	1.1
PSB-Sample1	6.4			−52, −52	2.4
PSB-Sample2	8.0			−64, −63	1.7
Chlorite schist					
PSB12-16		7.4		−50, −50	1.5
Continental basement/metasediments					
PSB12-12				−47, −48	1.3
PSB12-13				−54, −51	−0.6
PSB12-14				−51, −49	0.8
PSB12-15				−54, −50	−1.2
St. Barthelemy					
Serpentinites					
SB12-1	10.4			−68, −68	0.2
SB12-2	9.2			−90, −91	n.d
SB12-3	9.4			−58, −56	n.d
SB12-4	n.d			−57, −57	n.d
Metasediments					
SB12-5				−49, −49	n.d
Rocca Canavese Zone (*Levone River sequence*)					
Serpentinites					
LV12-4	5.6			−96, −97	0.5
LV12-5	6.2			−99, −101	1.0
LV12-6	5.7			−81, −78	0.8
Omphacitite					
LV12-3			7.1, 7.2	BDL	−0.4
Canavese Zone					
Serpentinites					
LV12-1	6.8			−89, −91	1.0
LV12-2	5.2			−86, −85	0.9

[a] Replicate δD analyses are given.

et al., 2008). δD values of sedimentary material have a large range of ~ −35 to −95‰ (e.g., Savin and Epstein, 1970; Yeh, 1980; Sharp, 2007) (Fig. 9). The measured δD values of the nearby metasedimentary and continental basement rocks in this study range from −54 to −47‰, higher

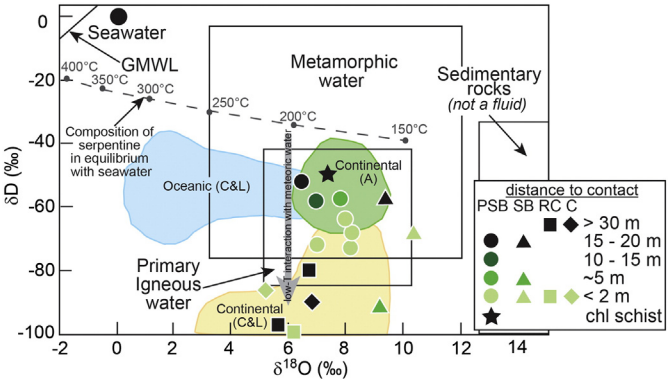

Fig. 9. Oxygen and hydrogen isotope composition of Punta Rossa (PSB; circles; chlorite schist = star), St. Barthelemy (SB; squares), Rocca Canavese (RC; squares), and Canavese (C; diamonds) serpentinites of varying distances to the contact with sedimentary units and/or continental basement. The δD and $\delta^{18}O$ values of various fluids/fluid sources are from Sharp (2007). Dashed gray line represents the isotopic composition of serpentine in equilibrium with seawater at a given temperature using the fractionation factors of Saccocia et al. (2009). Low-temperature post-serpentinization interaction with meteoric water can lower the δD values of serpentine (O'Hanley, 1996; Kyser et al., 1999), depicted by thick, gray arrow. δD and $\delta^{18}O$ values for serpentinites from continental and oceanic settings from Wenner and Taylor (1973, 1974). A = antigorite; L = lizardite; C = chrysotile.

than those of the serpentinites. With increasing metamorphic grade, sediments are hypothesized to preferentially lose D with the residual slab becoming progressively lower in δD values (Shaw et al., 2008, 2012). δD values of possible crustal fluid sources were only measured on a handful of samples (n = 5) (Table 5), therefore, sources of lower δD values may exist, but were not measured. The low δD values may also reflect interaction along the serpentinite–sediment interface with a metamorphic fluid derived from deeper in the subduction channel and no longer recorded in the rock record. An alternate possibility is that the low δD values are from the contribution of secondary minerals. Hydrogen isotope analyses are of bulk powders, therefore the δD values reflect the isotopic composition of all mineral phases in the rock, including secondary talc and/or amphibole. In the Punta Rossa unit, the samples with the lowest δD values are those containing talc. Samples from the Canavese and Rocca Canavese units contain amphibole. Late-stage talc and/or amphibole may have undergone interaction with meteoric water lowering the bulk δD values.

6.2.2. Trace element data

In general, the concentrations of Pb, Ba, Cs, U, and Rb increase towards the serpentinite and sediment/continental basement interface (Fig. 11). These trends are clearest in the Punta Rossa unit, where the present-day relative distances between the serpentinites and the sediments and/or continental basement have been maintained throughout the Alpine deformation history. This conclusion is supported by the detailed structural and lithostratigraphic study reported in Beltrando et al. (2012), showing that the different pre-Alpine marker layers can be followed continuously across the hinges of Alpine faults. However, note that the absolute distances are likely to have been modified due to deformation-induced

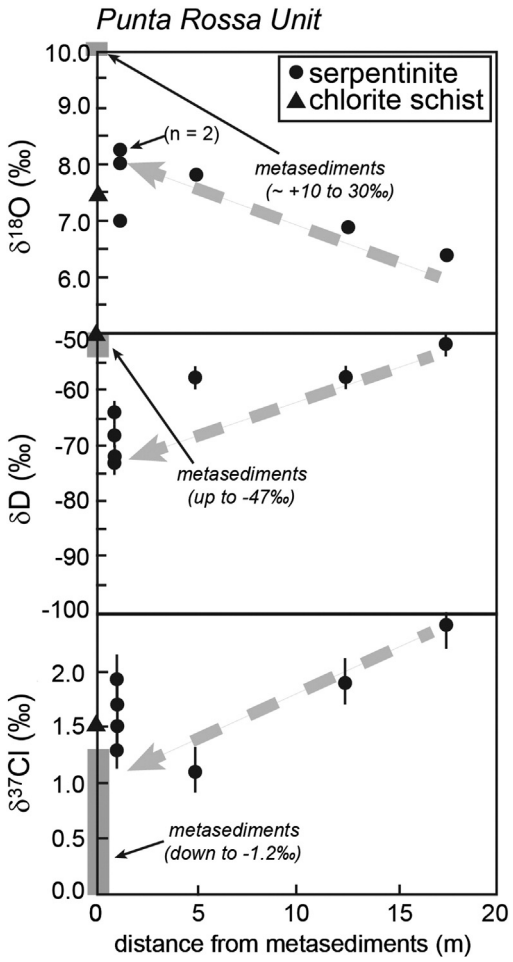

Fig. 10. Oxygen, hydrogen, and chlorine isotope compositions of the Punta Rossa serpentinite (circle) and chlorite schist (triangle) versus distance from the contact with the continental basement and/or metasediments. Gray boxes highlight the δD and $\delta^{37}Cl$ values of adjacent crustal material from this study. The gray box showing the range of $\delta^{18}O$ values for metasediments is from Sharp (2007). Thick gray arrow highlights the trend of increasing $\delta^{18}O$, decreasing δD, and decreasing $\delta^{37}Cl$ values with decreasing distance to the contact with the metasediments.

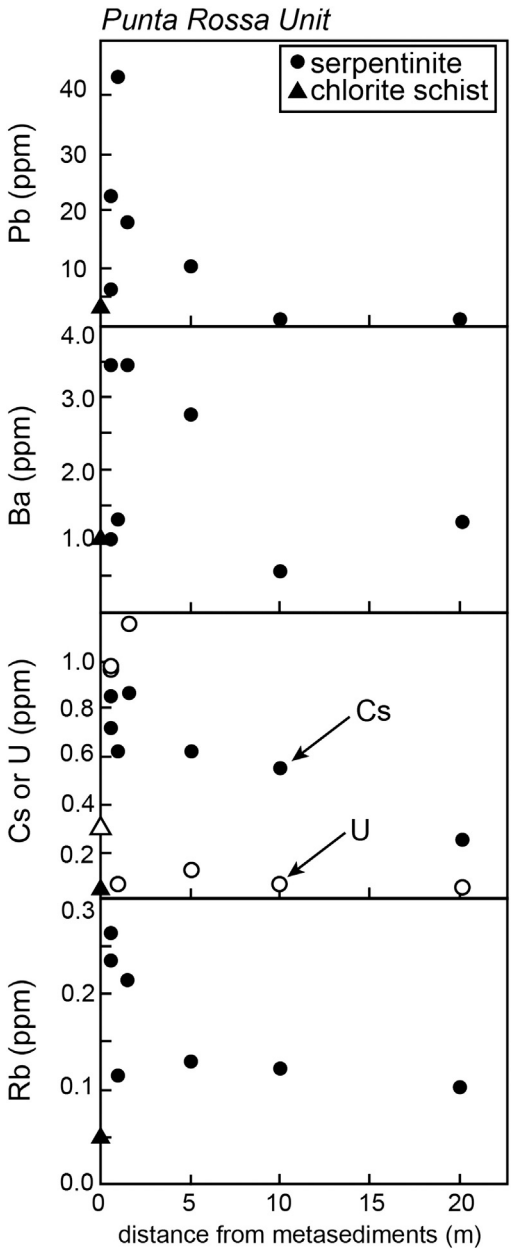

Fig. 11. Bulk trace element concentrations (Pb, Ba, Cs, U, and Rb) of the Punta Rossa serpentinite (circle) and chlorite schist (triangle) versus distance from the contact with the continental basement and/or metasediments. Open symbols are uranium.

recrystallization during the documented multi-stage folding, hence potentially steepening the compositional gradients documented in this study. No such tight control on the relative position of the studied serpentinites with respect to the surrounding lithologies throughout their Alpine evolution is available for the other localities that have been studied here. In the Canavese Zone, the Pesmonte serpentinite, locally directly in contact with radiolarian cherts, is bounded on all sides by post-metamorphic faults (Fig. 3E; Beltrando et al., in press), which have likely modified the original relative position of ultramafic rocks and post-rift cover. In Saint Barthelemy, the interface between serpentinites and post-rift cover is marked by a 2 m thick late-metamorphic fault zone. Although no significant motion can be inferred along this structure, due to the consistency of the lithostratigraphy observed in this area (Baldelli et al., 1983), its activity possibly resulted in late-stage modifications of the serpentinite-cover interface. Furthermore, within the Rocca Canavese unit, the relative distance of samples LV12-3, 4 and 5 with respect to the neighboring orthogneiss can tracked only as far back as the high-pressure metamorphic stages, when the main field fabric was formed (Pognante, 1989). Therefore, significant modifications of the relative distance between the studied samples and the surrounding orthogneisses prior to that fabric-forming stage cannot be assessed. Considering the limitations listed above, our discussion on the spatial compositional trends is largely restricted to the Punta Rossa serpentinite. Pb, Ba, Cs, U, and Rb are all enriched in crustal material compared to ultramafic material (e.g., Wedepohl, 1995; Rudnick and Gao, 2004) and therefore likely document increased interaction between sedimentary derived fluids and serpentinites near the interface. Enrichments in Cs, U, and Pb are common in subducted serpentinites and increased concentrations have previously been attributed to interaction with sediments in a subduction channel (Deschamps et al., 2013; Lafay et al., 2013). Pb isotope work on serpentinites also suggests that Pb enrichments may be derived from Pb-bearing fluids released by sediment dehydration during subduction (Deschamps et al., 2012). Pelletier et al. (2008) also note a distinct increase in Pb concentration in serpentinites nearest the contact with crustal material and interpret this increase as interaction with crustal derived fluids. Although Cs and Pb concentrations are high in serpentinites from passive margins (Kodolányi et al., 2012), they are not as enriched as in the Alpine serpentinites studied in this work (Fig. 6C and D). Bulk rock trace element data on serpentinites from the Galicia and Newfoundland margins are limited. The limited data available show no consistent increase in Pb, Ba, Cs, U, and Rb near the interface with the overlaying

units, with the possible exception of U and Ba (Hébert et al., 2001; Kodolányi et al., 2012). However, U enrichments may be due to seafloor weathering and/or carbonate-hosted U (Kodolányi et al., 2012 and references therein). Despite the limited data, we speculate that these geochemical trends are unlikely a seafloor feature, but rather the Pb, Ba, Cs, U, and Rb enrichment occurred due to metasomatism from sedimentary derived fluids during subduction and/or exhumation of the ultramafic rocks. The relatively impermeable nature of the serpentinites limits interaction to only the outer few meters of the serpentinite body, as is also noted in other geochemical transect studies of serpentinites (Pelletier et al., 2008) (Fig. 11).

6.3. Analog to the slab–mantle interface

Although we interpret the serpentinites from the localities described in this work to be of abyssal origin in a hyper-extended rifted setting, largely preserving the relative position with respect to the surrounding rocks in the Punta Rossa unit, Saint Barthelemy area and Canavese Zone, their interface with meta-pelites and orthogneisses is analogous to the subducted sediment–mantle wedge interface. At the slab–mantle interface, rocks of different lithologies undergo metasomatism due to steep geochemical gradients, as well as, mechanical mixing (e.g., Bebout and Barton, 2002; Bebout, 2007). Much work has focused on exhumed subduction complexes, as representatives of this interface, to investigate elemental mobility and transfer from the subducting slab into the overlying mantle (e.g., Sorensen et al., 1997; Bebout and Barton, 2002; King et al., 2003; Breeding et al., 2004; Marschall et al., 2006; Bebout, 2007). Work on HP and UHP metamafic and metasedimentary rocks has shown mobility of LILE (K, Rb, Cs, Ba, Sr), U, Pb, Th, and B (see Bebout, 2007, 2012 and references therein). Experimental work suggests the ability of subduction zone fluids to transport LILE, Pb, Th, U, Sr, and LREE (Kessel et al., 2005). The enrichments in Ba, Rb, U, Cs, and Pb in bulk serpentinites from the Punta Rossa unit near the interface with crustal materials reflect this transport of fluids from the sedimentary unit into the serpentinites (Fig. 11). It is interesting to note the influx of these elements into the serpentinite, rather than loss of these elements by fluids fluxing along the contact boundary. This is in contrast to other work which has noted limited elemental exchange between adjacent ultramafic and sedimentary materials in subduction mélange (Breeding et al., 2004). The preservation of this chemical gradient is evidence for limited involvement of externally derived fluids fluxing along the boundary.

Of particular interest are metasomatic blackwall zones between serpentinites and crustal material. These so-called “hybrid” rocks are commonly observed in exhumed subduction complexes and in seafloor settings (e.g., Bebout and Barton, 2002; King et al., 2003; Breeding et al., 2004; Boschi et al., 2006; Spandler et al., 2008; Miller et al., 2009; Marocchi et al., 2010). These rocks are the products of intense metasomatism due to the juxtaposition of chemically disparate rocks and are commonly monomineralic, consisting of solely of talc or chlorite, for example. These zones are a reaction front and therefore form an entirely new bulk composition with no sedimentary or igneous equivalent (e.g., Miller et al., 2009). The REE pattern of the chlorite schist rimming the Punta Rossa serpentinite is identical to REE patterns of chlorite schists from New Caledonia (Spandler et al., 2008). It is not possible to determine if the metasomatism is a relict seafloor feature or formed during subduction or exhumation of the margin. Previous workers have noted the potential, and largely overlooked, role hybrid rocks have as carriers of LILE and water into subduction zones (Spandler et al., 2008; Miller et al., 2009). We note that although the water content in the analyzed chlorite schist is high, the LILE concentrations are lower than at the serpentinite near the contact.

7. Conclusions

The major and trace element geochemistry of the Canavese, Rocca Canavese, St. Barthelemy and Punta Rossa bulk serpentinites, as well as the composition of relict spinels and pyroxene from the Rocca Canavese, are consistent with small to moderate melt depletion of subcontinental mantle. Oxygen isotope data supports low-temperature serpentinization (between 150 and 200 °C) by seawater at or near the seafloor. These geochemical data support lithostratigraphic evidence of exhumation of a hyper-extended rifted margin of the Alpine Tethys for the Canavese, St. Barthelemy and Punta Rossa serpentinites. However, we note that the trace element and stable isotope geochemistry of serpentinites adjacent to crustal material may be modified by fluid–rock interaction during subduction and exhumation. Pb, Ba, Cs, U, and Rb all show enrichments within the serpentinite closest to the contact with metasediments. $\delta^{18}O$ values increase and $\delta^{37}Cl$ values decrease also near the contact implying an influx of sedimentary derived fluid. Care should be taken when interpreting the geochemistry of serpentinites adjacent to crustal material as the bulk chemistry may be modified by fluid interaction. However, these observations provide information regarding the mobility of these elements during subduction and their sequestration into serpentinites. Serpentinites serve as hosts for Pb, Ba, Cs, U, and Rb up to at least blueschist facies (~375 °C). This is consistent with observations by Lafay et al. (2013) who note the retention of Cs up to 360 °C, or possibly even higher (≥400 °C) (Deschamps et al., 2010, 2011). Deschamps et al. (2011, 2010) also note the retention of U, Pb, Sr and Ba in serpentinites at high temperatures (≥400 °C). Despite the enrichment of LILE (Rb, Cs) in the chlorite schist and the overlooked potential of “hybrid” rocks as carriers of LILE into subduction zones, we note that the concentrations of these elements are significantly higher in the exceedingly more abundant serpentinite.

Acknowledgments

The authors acknowledge T. Larson for help with stable isotope analyses, N. Miller and E. Marshall for help with LA-ICP-MS work, and M. Gevedon for help with electron microprobe work. The authors gratefully thank L. Reisberg for editorial handling and helpful comments and thorough and constructive reviews by G. Manatschal and F. Deschamps, which greatly improved this contribution. This work was partially supported by funds from the Rosamond Allen Haertlein and Jeanne Allen Ferrin Faculty Fund at the Jackson School of Geosciences.

References

Afilhado, A., Matias, L., Shiobara, H., Hirn, A., Victor, L.M., Shimamura, H., 2008. From unthinned continent to ocean: the deep structure of the West Iberia passive continental margin at 38°N. Tectonophysics 458, 9–50.

Agranier, A., Lee, C.-T.A., Li, Z.-X.A., Leeman, W.P., 2007. Fluid-mobile element budgets in serpentinized oceanic lithospheric mantle: insights from B, As, Li, Pb, PGEs and Os isotopes in the Feather River Ophiolite, California. Chem. Geol. 245, 230–241.

Agrinier, P., Mével, C., Girardeau, J., 1988. Hydrothermal alteration of the peridotites cored at the ocean/continent boundary of the Iberian margin: petrologic and stable isotope evidence. Proc. Ocean Drill. Program Sci. Results 103, 225–234.

Agrinier, P., Cornen, G., Beslier, M.-O., 1996. Mineralogical and oxygen isotopic features of the serpentinites recovered from the ocean/continent transition in the Iberia Abyssal Plain. In: Whitmarsh, R.B., Sawyer, D.S., Klaus, A., Masson, D.G. (Eds.), Proceedings of the Ocean Drilling Program, Scientific Results. Ocean Drilling Program, College Station, TX, pp. 541–552.

Alt, J.C., Shanks, W.C., 2006. Stable isotope compositions of serpentinite seamounts in the Mariana forearc: serpentinization processes, fluid sources and sulfur metasomatism. Earth Planet. Sci. Lett. 242, 272–285.

Anselmi, B., Mellini, M., Viti, C., 2000. Chlorine in the Elba, Monti Livornesi and Murlo serpentines: evidence for sea–water interaction. Eur. J. Mineral. 12 (1), 137–146.

Baldelli, E., Dal Piaz, G.V., Polino, R., 1983. Le quarziti a manganese e cromo di Varenche-St. Barthelemy, una sequenza di copertura oceanica delia falda piemontese. Ofioliti 8, 208–221.

Barnes, J.D., Sharp, Z.D., 2006. A chlorine isotope study of DSDP/ODP serpentinized ultramafic rocks: insights into the serpentinization process. Chem. Geol. 228, 246–265.

Barnes, J.D., Selverstone, J., Sharp, Z.D., 2006. Chlorine chemistry of serpentinites from Elba, Italy, as an indicator of fluid source and subsequent tectonic history. Geochem. Geophys. Geosyst. 7, Q08015. http://dx.doi.org/10.1029/2006GC001296.

Barnes, J.D., Sharp, Z.D., Fischer, T.P., 2008. Chlorine isotope variations across the Izu–Bonin–Mariana arc. Geology 36, 883–886.

Barnes, J.D., Paulick, H., Sharp, Z.D., Bach, W., Beaudoin, G., 2009. Stable isotope ($d^{18}O$, dD, $d^{37}Cl$) evidence for multiple fluid histories in mid-Atlantic abyssal peridotites (ODP Leg 209). Lithos 110, 83–94.

Barnes, J.D., Eldam, R., Lee, C.-T.A., Errico, J.C., Loewy, S.L., Cisneros, M., 2013. Petrogenesis of serpentinites from the Franciscan Complex, western California, USA. Lithos 178, 143–157.

Bearth, P., 1967. Die Ophiolithe der Zone von Zermatt-Saas Fee. Beitr. Geol. Karte Schweiz. 132, 1–130.

Bebout, G.E., 2007. Metamorphic chemical geodynamics of subduction zones. Earth Planet. Sci. Lett. 260, 373–393.

Bebout, G.E., 2012. Ch. 9.Metasomatism in subduction zones of oceanic slabs, mantle wedges, and the slab–mantle interface. In: Harlov, D., Austrheim, H. (Eds.), Metasomatism and the Chemical Transformation of Rock. Springer-Verlag, Berlin Heidelberg, pp. 289–349.

Bebout, G.E., Barton, M.D., 2002. Tectonic and metasomatic mixing in a high-T, subduction-zone melange: insights into the geochemical evolution of the slab–mantle interface. Chem. Geol. 187, 79–106.

Bebout, G.E., Ryan, J.G., Leeman, W.P., Bebout, A.E., 1999. Fractionation of trace elements by subduction-zone metamorphism—effect of convergent-margin thermal evolution. Earth Planet. Sci. Lett. 171, 63–81.

Beltrando, M., Rubatto, D., Compagnoni, R., Lister, G., 2007. Was the Valaisan basin floored by oceanic crust? Evidence of Permian magmatism in the Versoyen unit (Valaisan Domain, NW Alps). Ofioliti 32, 85–99.

Beltrando, M., Compagnoni, R., Lombardo, B., 2010a. (Ultra-) High-pressure metamorphism and orogenesis: an Alpine perspective. Gondwana Res. 18, 147–166. http://dx.doi.org/10.1016/j.gr.2010.01.009.

Beltrando, M., Rubatto, D., Manatschal, G., 2010b. From passive margins to orogens: the link between ocean–continent transition zones and (ultra)high-pressure metamorphism. Geology 38, 559–562.

Beltrando, M., Frasca, G., Compagnoni, R., Vitale Brovarone, A., 2012. The Valaisan controversy revisited: multi-stage folding of a Mesozoic hyper-extended margin in the Petit St. Bernard Pass area (western Alps). Tectonophysics 579, 17–36.

Beltrando, M., Manatschal, G., Mohn, G., Dal Piaz, G.V., Vitale Brovarone, A., Masini, E., 2014. Recognizing remnants of magma-poor rifted margins in high-pressure orogenic belts: The alpine case study. Earth-Sci. Rev. 131, 88–115. http://dx.doi.org/10.1016/j.earscirev.2014.01.001.

Beltrando, M., Compagnoni, R., Ferrando, S., Mohn, G., Frasca, G., Odasso, N., Vukmanovič, Z., Masini, E., Beltrando, M., 2014. Crustal thinning and mantle exhumation in the Levone area (Southern Canavese Zone, Western Alps). In: Manatschal, G., Mohn, G. (Eds.), A Field Guide Across the Margins of Alpine Tethys. J. Virtual Explor (in press).

Biino, G., Compagnoni, R., 1989. The Canavese Zone between the Serra d'Ivrea and the Dora Baltea River (western Alps). Eclogae Geol. Helv. 82, 413–427.

Bill, M., O'Dogherty, L., Guex, J., Baumgartner, P.O., Masson, H., 2001. Radiolarite ages in Alpine–Mediterranean ophiolites. Constraints on the oceanic spreading and the Tethys–Atlantic connection. Geol. Soc. Am. Bull. 113, 129–143.

Bodinier, J.-L., Godard, M., 2005. Orogenic, ophiolitic, and abyssal peridotites. In: Carlson, R.W. (Ed.), The Mantle and Core, Treatise on Geochemistry. Elsevier Science, pp. 103–170.

Bonifacie, M., Busigny, V., Mével, C., Philippot, P., Agrinier, P., Jendrzejewski, N., Scambelluri, M., Javoy, M., 2008. Chlorine isotopic composition in seafloor serpentinites and high-pressure metaperidotites. Insights into oceanic serpentinization and subduction processes. Geochim. Cosmochim. Acta 72, 126–139.

Boschi, C., Früh-Green, G.L., Delacour, A., Karson, J.A., Kelley, D.S., 2006. Mass transfer and fluid flow during detachment faulting and development of an oceanic core complex, Atlantis Massif (MAR 30 N). Geochem. Geophys. Geosyst. 7, Q01004. http://dx.doi.org/10.1029/2005GC001074.

Boschi, C., Bonatti, E., Ligi, M., Brunelli, D., Dallai, L., D'Orazio, M., Früh-Green, G., Tonarini, S., Barnes, J.D., Bedini, R., 2013. A 10 Ma year old window into deep hydrothermal circulation at the Vema Fracture Zone (11°N, MAR). Lithos 178, 3–23.

Bousquet, R., Goffé, B., Vidal, O., Oberhänsli, R., Patriat, M., 2002. The tectonometamorphic history of the Valaisan domain from the Western to the Central Alps: new constraints on the evolution of the Alps. Geol. Soc. Am. Bull. 114, 207–225.

Breeding, C.M., Ague, J.J., Bröcker, M., 2004. Fluid–metasedimentary rock interactions in subduction-zone mélange: implications for the chemical composition of arc magmas. Geology 32, 1041–1044.

Burkhard, D.J.M., O'Neil, J.R., 1988. Contrasting serpentinization processes in the eastern Central Alps. Contrib. Mineral. Petrol. 99, 498–506.

Carta Geologica d'Italia/APAT, S.G., 2006. Foglio 091 Châtillon della Carta Geologica d'Italia alla scala 1:50.000. ATI: SEL.CA., System Cart, LAC. Coordinatore Scientifico: Dal Piaz, G.V.

Cartwright, I., Barnicoat, A.C., 1999. Stable isotope geochemistry of Alpine ophiolites: a window to ocean-floor hydrothermal alteration and constraints on fluid-rock interaction during high-pressure metamorphism. Int. J. Earth Sci. 88 (2), 219–235.

Coward, M.P., Dietrich, D., 1989. Alpine tectonics — an overview. In: Coward, M.P., Dietrich, D., Park, R.G. (Eds.), Alpine Tectonics, Special Publication. Geological Society, London, pp. 1–29.

Dal Piaz, G.V., 1967. Le "granatiti" (rodingiti l.s.) nelle serpentiniti delle Alpi occidentali italiane. Mem. Soc. Geol. Ital. 6, 267–313.

Dal Piaz, G.V., 1969. Nuovo affioramento di quarziti e scisti a piemontite in Valle d'Aosta. Boll. Soc. Geol. Ital. 88, 613–619.

Dal Piaz, G.V., 1999. The Austroalpine–Piedmont nappe stack and the puzzle of Alpine Tethys. Mem. Sci. Geol. Padova 51, 155–176.

Dal Piaz, G.V., 2010. The Italian Alps: a journey across two centuries of Alpine geology. J. Virtual Explor. 36. http://dx.doi.org/10.3809/jvirtex.2010.00234.

Debret, B., Andreani, M., Godard, M., Nicollet, C., Schwartz, S., Lafay, R., 2013. Trace element behavior during serpentinization/de-serpentinization of an eclogitized oceanic lithosphere: a LA-ICPMS study of the Lanzo ultramafic massif (Western Alps). Chem. Geol. 357, 117–133.

Deschamps, F., Guillot, S., Godard, M., Chauvel, C., Andreani, M., Hattori, K., 2010. In situ characterization of serpentinites from forearc mantle wedges: timing of serpentinization and behavior of fluid-mobile elements in subduction zones. Chem. Geol. 269, 262–277.

Deschamps, F., Guillot, S., Godard, M., Andreani, M., Hattori, K., 2011. Serpentinites act as sponges for fluid-mobile elements in abyssal and subduction zone environments. Terra Nova 23 (3), 171–178.

Deschamps, F., Godard, M., Guillot, S., Chauvel, C., Andreani, M., Hattori, K., Wunder, B., France, L., 2012. Behavior of fluid-mobile elements in serpentines from abyssal to subduction environments: examples from Cuba and Dominican Republic. Chem. Geol. 312–313, 93–117.

Deschamps, F., Godard, M., Guillot, S., Hattori, K., 2013. Geochemistry of subduction zone serpentinites: A review. Lithos 178, 96–127.

Dewey, J.F., Pitman, W.C., Ryan, W.B.F., Bonnin, J., 1973. Plate tectonics and the evolution of the Alpine system. Geol. Soc. Am. Bull. 84, 3,137–3,180.

Eggenkamp, H.G.M., 1994. The Geochemistry of Chlorine Isotopes(Ph.D. Thesis) Universiteit Utrecht, (151 pp.).

Elter, G., 1971. Schistes lustrés et ophiolites de la zone piémontaise entre Orco and Doire Baltée (Alpes Graies). Hypothèses sur l'origine des ophiolites. Géol. Alpine (Grenoble) 47, 147–169.

Elter, G., Elter, P., Sturani, C., Weidmann, M., 1966. Sur la prolongation du domaine ligure de l'Apennin dans le Monferrat et les Alpes et sur l'origine de la Nappe de la Simme s. l. des Préalpes romandes et chablaisiennes. Arch. Sci. (Genève) 19, 279–377.

Evans, B., 2004. The serpentinite multisystem revisited: chrysotile is metastable. Int. Geol. Rev. 46, 479–506.

Federico, L., Crispini, L., Scambelluri, M., Capponi, G., 2007. Ophiolite mélange zone records exhumation in a fossil subduction channel. Geology 35, 499–502.

Ferrando, S., Bernoulli, D., Compagnoni, R., 2004. The Canavese zone (internal Western Alps): a distal margin of Adria. Schweiz. Mineral. Petrogr. Mitt. 84, 237–256.

Frisch, W., 1979. Tectonic progradation and plate tectonic evolution of the Alps. Tectonophysics 60, 121–139.

Froitzheim, N., Eberli, G.P., 1990. Extensional detachment faulting in the evolution of a Tethys passive continental margin, Eastern Alps, Switzerland. Geol. Soc. Am. Bull. 102, 1297–1308.

Froitzheim, N., Manatschal, G., 1996. Kinematics of Jurassic rifting, mantle exhumation, and passive margin formation in the Austroalpine and Penninic nappes (eastern Switzerland). Geol. Soc. Am. Bull. 108, 1120–1133.

Früh-Green, G.L., Weissert, H., Bernoulli, D., 1990. A multiple fluid history recorded in Alpine ophiolites. J. Geol. Soc. 147, 959–970.

Früh-Green, G.L., Plas, A., Lécuyer, C., 1996. Petrologic and stable isotope constraints on hydrothermal alteration and serpentinization of the EPR shallow mantle at Hess Deep (Site 895). In: Mével, C., Gillis, K.M., Allan, J.F., Meyer, P.S. (Eds.), Proc. ODP, Sci. Results. Ocean Drilling Program, College Station, TX, pp. 255–287.

Früh-Green, G.L., Scambelluri, M., Vallis, F., 2001. O–H isotope ratios of high pressure ultramafic rocks: implications for fluid sources and mobility in the subducted hydrous mantle. Contrib. Mineral. Petrol. 141 (2), 145–159.

Galvez, M.E., Beyssac, O., Martinez, I., Benzerara, K., Chaduteau, C., Malvoisin, B., Malavieille, J., 2013. Graphite formation by carbonate reduction during subduction. Nat. Geosci. 6, 473–477.

Gerya, T.V., Stöckhert, B., Perchuk, A.L., 2002. Exhumation of high pressure metamorphic rocks in a subduction channel-a numerical simulation. Tectonics 21. http://dx.doi.org/10.1029/2002TC001406.

Groppo, C., Compagnoni, C., 2007. Metamorphic veins from the serpentinites of the Piemonte Zone, western Alps, Italy: a review. Periodico Mineral. 76, 127–153.

Guillot, S., Hattori, K., Agard, P., Schwartz, S., Vidal, O., 2009. Exhumation processes in oceanic and continental subduction contexts: a review. In: Lallemand, S., Funiciello, F. (Eds.), Subduction Zone Geodynamics (Frontiers in Earth Sciences). Springer Berlin, Heidelberg, pp. 175–205.

Hattori, K.H., Guillot, S., 2003. Volcanic fronts form as a consequence of serpentinite dehydration in the forearc mantle wedge. Geology 31, 525–528.

Hattori, K.H., Guillot, S., 2007. Geochemical character of serpentinites associated with high- to ultrahugh-pressure metamorphic rocks in the Alps, Cuba, and the Himalayas: recycling of elements in subduction zones. Geochem. Geophys. Geosyst. 8.

Hawkesworth, C.J., Gallagher, K., Hergt, J.M., McDermott, F., 1993. Mantle and slab contribution in arc magmas. Annu. Rev. Earth Planet. Sci. 21, 175–204.

Hébert, R., Gueddari, K., Laflèche, M.R., Beslier, M.-O., Gardien, V., 2001. Petrology and geochemistry of exhumed peridotites and gabbros at non-volcanic margins: ODP Leg 173 West Iberia ocean-continent transition zone. In: Wilson, R.C.L., Whitmarsh, R.B., Taylor, B., Froitzheim, N. (Eds.), Non-Volcanic Rifting of Continental Margins: A Comparison of Evidence from Land and Sea. Geological Society Special Publications, London, pp. 161–189.

Hellebrand, E., Snow, J.E., Hoppe, P., Hofmann, A.W., 2002. Garnet field melting and late stage refertilization in residual abyssal peridotites from the Central Indian Ridge. J. Petrol. 43, 2305–2338.

Hellstrom, J., Paton, C., Woodhead, J., Hergt, J., 2008. Iolite: software for spatially resolved LA-(quad and MC) ICPMS analysis. Mineralogical Association of Canada Short Course Series 40, pp. 343–348.

Ishii, T., Robinson, P.T., Maekawa, H., Fiske, R., 1992. Petrological studies of peridotites from diapiric serpentinite seamounts in the Izu–Ogasawara–Mariana forearc. In: Fryer, P., Pearce, J.A., Stokking, L.B. (Eds.), Proc. of the Ocean Drilling Program, Sci. Results. Ocean Drilling Program, College Station, TX, pp. 445–485.

Jagoutz, E., Palme, H., Baddenhausen, H., Blum, K., Cendales, M., Dreibus, G., Spettel, B., Lorenz, V., Vanke, H., 1979. The abundance of major, minor and trace elements in the earth's mantle as derived from primitive ultramafic nodules. Geochim. Cosmochim. Acta 11, 2031–2050.

John, T., Layne, G.D., Haase, K.M., Barnes, J.D., 2010. Chlorine isotope evidence for crustal recycling into the Earth's mantle. Earth Planet. Sci. Lett. 298, 175–182.

John, T., Scambelluri, M., Frische, M., Barnes, J.D., Bach, W., 2011. Dehydration of subducting serpentinite: implications for halogen mobility in subduction zones and the deep halogen cycle. Earth Planet. Sci. Lett. http://dx.doi.org/10.1016/j.epsl.2011.05.038.

Johnson, K.T.M., Dick, H.J.B., Shimizu, N., 1990. Melting in the oceanic upper mantle: an ion microprobe study of diopsides in abyssal peridotites. J. Geophys. Res. 95, 2661–2678.

Kessel, R., Schmidt, M.W., Ulmer, P., Pettke, T., 2005. Trace element signature of subduction-zone fluids, melts and supercritical liquids at 120–180 km depth. Nature 437, 724–727.

King, R.L., Kohn, M.J., Eiler, J.M., 2003. Constraints on the petrological structure of the subduction zone slab–mantle interface from Franciscan Complex exotic ultramafic blocks. Geol. Soc. Am. Bull. 115, 1097–1109.

Kodolányi, J., Pettke, T., Spandler, C., Kamber, B.S., Gméling, K., 2012. Geochemistry of ocean floor and fore-arc serpentinites: constraints on the ultramafic input to subduction zones. J. Petrol. 53, 235–270.

Kyser, T.K., Kerrich, R., 1991. Retrograde exchange of hydrogen isotopes between hydrous minerals and water at low temperatures. In: Taylor, H.P., O'Neil, J.R., Kaplan, I.R. (Eds.), Stable Isotope Geochemistry, A tribute to Samuel Epstein. Geochem. Soc. Spec. Pub. , pp. 409–422.

Kyser, T.K., O'Hanley, D.S., Wicks, F.J., 1999. The origin of fluids associated with serpentinization processes: Evidence from stable-isotope compositions. Can. Mineral. 37, 223–237.

Lafay, R., Deschamps, F., Schwartz, S., Guillot, S., Godard, M., Debret, B., Nicollet, C., 2013. High-pressure serpentinites, a trap-and-release system controlled by metamorphic conditions: example from the Piedmont zone of the western Alps. Chem. Geol. 343, 38–54.

Lagabrielle, Y., Nervo, R., Polino, R., Dutto, F., 1982. Sedimentary cover of some ophiolites of Cottian Alps. Ofioliti 2 (3), 339–350.

Lemoine, M., Steen, D., Vuagnat, M., 1970. Sur le problème stratigraphique des ophiolites piémontaises et des roches sédimentaires associées: observations dans le massif de Chabrière en Haute- Ubaye (Basses-Alpes, France). C. R. Soc. Phys. Hist. Nat. Geneve N. S. 5, 44–59.

Li, X.P., Rahn, M.K., Bucher, K., 2004. Serpentinites of the Zermatt–Saas ophiolite complex and their texture evolution. J. Metamorph. Geol. 22, 159–177.

Loprieno, A., Bousquet, R., Bucher, S., Ceriani, S., Dalla Torre, F.H., Fügenschuh, B., Schmid, S.M., 2011. The Valais units in Savoy (France): a key area for understanding the palaeogeography and the tectonic evolution of the Western Alps. Int. J. Earth Sci. 100, 963–992.

Magenheim, A.J., Spivack, A.J., Volpe, C., Ransom, B., 1994. Precise determination of stable chlorine isotopic ratios in low-concentration natural samples. Geochim. Cosmochim. Acta 58 (14), 3117–3121.

Malatesta, C., Gerya, T., Scambelluri, M., Federico, L., Crispini, L., Capponi, G., 2012. Intraoceanic subduction of "heterogeneous" oceanic lithosphere in narrow basins: 2D numerical modeling. Lithos 140–141, 234–251.

Malvoisin, B., Chopin, C., Brunet, F., Galvez, M.E., 2012. Low-temperature wollastonite formed by carbonate reduction: a marker of serpentinite redox conditions. J. Petrol. 53, 159–176.

Manatschal, G., 2004. New models for evolution of magma-poor rifted margins based on a review of data and concepts from West Iberia and the Alps. Int. J. Earth Sci. 93, 432–466.

Manatschal, G., Müntener, O., 2009. A type sequence across an ancient magma-poor ocean–continent transition: the example of the western Alpine Tethys ophiolite. Tectonophysics 473, 4–19.

Manatschal, G., Sauter, D., Karpoff, A.M., Masini, E., Mohn, G., Lagabrielle, Y., 2011. The Chenaillet Ophiolite in the French/Italian Alps: an ancient analogue for an Oceanic Core Complex? Lithos 124, 169–184.

Marocchi, M., Hermann, J., Tropper, P., Bargossi, G.M., Mair, V., 2010. Amphibole and phlogopite in "hybrid" metasomatic bands monitor trace element transfer at the interface between felsic and ultramafic rocks (Eastern Alps, Italy). Lithos 117, 135–148.

Marschall, H.R., Altherr, R., Ludwig, T., Kalt, A., Gméling, K., Kasztovszky, Z., 2006. Partitioning and budget of Li, Be and B in high-pressure metamorphic rocks. Geochim. Cosmochim. Acta 70, 4750–4769.

Masson, H., 2002. Ophiolites and other (ultra)basic rocks from theWest-Central Alps: new data for a puzzle. Bull. Soc. Vaudoise Sci. Nat. 88, 263–276.

Mattey, D., Lowry, D., Macpherson, C., 1994. Oxygen isotope composition of mantle peridotite. Earth Planet. Sci. Lett. 128, 231–241.

McDonough, W.F., Sun, S.S., 1995. The composition of the Earth. Chem. Geol. 120, 223–253.

Miller, D.P., Marschall, H.R., Schumacher, J.C., 2009. Metasomatic formation and petrology of blueschist-facies hybrid rocks from Syros (Greece): implications for reactions at the slab–mantle interface. Lithos 107, 53–67.

Mohn, G., Manatschal, G., Müntener, O., Beltrando, M., Masini, E., 2010. Unravelling the interaction between tectonic and sedimentary processes during lithospheric thinning in the Alpine Tethys margins. Int. J. Earth Sci. 99 (Supplement 1), 75–101.

Müntener, O., Piccardo, G.B., 2003. Melt migration in ophiolitic peridotites: the message from Alpine–Apennine peridotites and implications for embryonic ocean basins. Geol. Soc. Lond. Spec. Publ. 218, 69–90.

Müntener, O., Manatschal, G., Desmurs, L., Pettke, T., 2010. Plagioclase peridotites in ocean–continent transitions: refertilized mantle domains generated by melt stagnation in the shallow mantle lithosphere. J. Petrol. 51, 255–294.

Niu, Y., 2004. Bulk-rock major and trace-element compositions of abyssal peridotites: implications for mantle melting, melt extraction and post-melting processes beneath mid-ocean ridges. J. Petrol. 45, 2423–2458.

O'Hanley, D.S., 1996. Serpentinites: Records of Tectonic and Petrological History. Oxford University Press, New York (277 pp.).

Parkinson, I.J., Pearce, J.A., 1998. Peridotites from the Izu–Bonin–Mariana forearc (ODP Leg 125): evidence for mantle melting and melt–mantle interaction in a supra-subduction zone setting. J. Petrol. 39, 1577–1618.

Paulick, H., Bach, W., Godard, M., De Hoog, J.C.M., Suhr, G., Harvey, J., 2006. Geochemistry of abyssal peridotites (Mid-Atlantic Ridge, 15°20′N, ODP Leg 209): implications for fluid/rock interaction in slow spreading environments. Chem. Geol. 234, 179–210.

Pelletier, L., Müntener, O., Kalt, A., Vennemann, T.W., Belgya, T., 2008. Emplacement of ultramafic rocks into the continental crust monitored by light and other trace elements: an example from the Geisspfad body (Swiss-Italian Alps). Chem. Geol. 255, 143–159.

Peron-Pinvidic, G., Manatschal, G., 2009. The final rifting evolution at deep magma-poor passive margins: a new point of view based on observations from Iberia-Newfoundland. Int. J. Earth Sci. 98. http://dx.doi.org/10.1007/s00531-008-0337-9.

Piccardo, G.B., 2010. The Lanzo peridotite massif, Italian Western Alps: Jurassic rifting of the Ligurian Tethys. Geol. Soc. Lond. Spec. Publ. 337, 47–69.

Piccardo, G.B., Zanetti, A., Müntener, O., 2007. Melt/peridotite interaction in the Southern Lanzo peridotite: field, textural and geochemical evidence. Lithos 94, 181–209.

Plank, T., Langmuir, C.H., 1993. Tracing trace elements from sediment input to volcanic output at subduction zones. Nature 362 (6422), 739–743.

Pognante, U., 1989. Lawsonite, blueschist and eclogite formation in the southern Sesia Zone (western Alps, Italy). Eur. J. Mineral. 1, 89–104.

Rampone, E., Borghini, G., 2008. Melt migration and intrusion in the Erro-Tobbio peridotites (Ligurian Alps, Italy): insights on magmatic processes in extending lithospheric mantle. Eur. J. Mineral. 20, 573–585.

Rosenbaum, G., Lister, G.S., 2005. The Western Alps from the Jurassic to Oligocene: spatio-temporal constraints and evolutionary reconstructions. Earth-Sci. Rev. 69, 281–306.

Rudnick, R.L., Gao, S., 2004. Composition of the continental crust. In: Holland, H.D., Turkekian, K.K. (Eds.), Treatise on Geochemistry, pp. 1–64.

Saccocia, P.J., Seewald, J.S., Shanks, W.C., 2009. Oxygen and hydrogen isotope fractionation in the serpentine-water and talc-water systems from 250° to 450 °C, 50 MPa. Geochim. Cosmochim. Acta 73, 6789–6804.

Sakai, R., Kusakabe, M., Noto, M., Ishii, T., 1990. Origin of waters responsible for serpentinization of the Izu–Ogasawara–Mariana forearc seamounts in view of hydrogen and oxygen isotope ratios. Earth Planet. Sci. Lett. 100, 291–303.

Savin, S.M., Epstein, S., 1970. The oyxgen and hydrogen isotope geochemistry of ocean sediments and shales. Geochim. Cosmochim. Acta 34, 43–63.

Savov, I.P., Ryan, J.G., D'Antonio, M., Kelley, K., Mattie, P., 2005. Geochemistry of serpentinized peridotites from the Mariana forearc Conical seamounts, ODP Leg 125: implications for the elemental recycling at subduction zones. Geochem. Geophys. Geosyst. 6.

Savov, I.P., Ryan, J.G., D'Antonio, M., Fryer, P., 2007. Shallow slab fluid release across and along the Mariana arc-basin system: insights from geochemistry of serpentinized peridotites from the Mariana fore arc. J. Geophys. Res. 112.

Scambelluri, M., Philippot, P., 2001. Deep fluids in subduction zones. Lithos 55, 213–227.

Scambelluri, M., Müntener, O., Ottolini, L., Pettke, T.T., Vannucci, R., 2004. The fate of B, Cl and Li in the subducted oceanic mantle and in the antigorite breakdown fluids. Earth Planet. Sci. Lett. 222, 217–234.

Schwartz, S., Allemand, P., Guillot, S., 2001. Numerical model of the effect of serpentinites on the exhumation of eclogitic rocks: insights from the Monviso ophiolitic massif (Western Alps). Tectonophysics 342, 193–206.

Selverstone, J., Sharp, Z.D., 2011. Chlorine isotope evidence for multicomponent mantle metasomatism in the Ivrea Zone. Earth Planet. Sci. Lett. 310, 429–440.

Selverstone, J., Sharp, Z.D., 2013. Chlorine isotope constraints on fluid-rock interactions during subduction and exhumation of the Zermatt–Saas ophiolite. Geochem. Geophys. Geosyst. 14, 4370–4391. http://dx.doi.org/10.1002/ggge.20269.

Sharp, Z.D., 1990. A laser-based microanalytical method for the *in situ* determination of oxygen isotope ratios of silicates and oxides. Geochim. Cosmochim. Acta 54, 1353–1357.

Sharp, Z.D., 2007. Principles of Stable Isotope Geochemistry. Pearson Prentice Hall, Upper Saddle River, NJ (344 pp.).

Sharp, Z.D., Barnes, J.D., 2004. Water soluble chlorides in massive seafloor serpentinites: a source of chloride in subduction zones. Earth Planet. Sci. Lett. 226, 243–254.

Sharp, Z.D., Atudorei, V., Durakiewicz, T., 2001. A rapid method for determination of hydrogen and oxygen isotope ratios from water and solid hydrous substances. Chem. Geol. 178, 197–210.

Sharp, Z.D., Barnes, J.D., Brearley, A.J., Chaussidon, M., Fischer, T.P., Kamenetsky, V.S., 2007. Chlorine isotope homogeneity of the mantle, crust and carbonaceous chondrites. Nature 446, 1062–1065.

Shaw, A.M., Hauri, E.H., Fischer, T.P., Hilton, D.R., Kelley, K.A., 2008. Hydrogen isotopes in Mariana arc melt inclusions: implications for subduction dehydration and the deep-Earth water cycle. Earth Planet. Sci. Lett. 275, 138–145.

Shaw, A.M., Hauri, E.H., Behn, M.D., Hilton, D.R., Macpherson, C.G., Sinton, J.M., 2012. Long-term preservation of slab signatures in the mantle inferred from hydrogen isotopes. Nat. Geosci. 5, 224–228.

Shipboard Scientific Party, 1998a. Leg 173 Introduction. In: Whitmarsh, R.B., Beslier, M.-O., Wallace, P.J. (Eds.), Proc. ODP, Init. Repts. Ocean Drilling Program, College Station, TX, pp. 7–23.

Shipboard Scientific Party, 1998b. Site 1068. In: Whitmarsh, R.B., Beslier, M.-O., Wallace, P. J. (Eds.), Proc. ODP, Init. Repts. Ocean Drilling Program, College Station, TX, pp. 163–218.

Skelton, A.D.L., Valley, J.W., 2000. The relative timing of serpentinisation and mantle exhumation at the ocean-continent transition, Iberia: constraints from oxygen isotopes. Earth Planet. Sci. Lett. 178, 327–338.

Sorensen, S.S., Grossman, J.N., Perfit, M.R., 1997. Phengite-hosted LILE enrichment in eclogite and related rocks: implications for fluid-mediated mass transfer in subduction zones and arc magma genesis. J. Petrol. 38, 3–34.

Spalla, M.I. and Zulbati, F., 2003. Structural and petrographic map of the southern Sesia-Lanzo Zone; Monte Soglio-Rocca Canavese, Western Alps, Italy. Memorie di Scienze Geologiche, 55: 119–127. 1 sheet, 1:10.000 scale.

Spandler, C., Hermann, J., Arculus, R., Mavrogenes, J., 2004. Geochemical heterogeneity and element mobility in deeply subducted oceanic crust; insights from high-pressure mafic rocks from New Caledonia. Chem. Geol. 206, 21–42.

Spandler, C., Hermann, J., Faure, K., Mavrogenes, J.A., Arculus, R.J., 2008. The importance of talc and chlorite "hybrid" rocks for volatile recycling through subduction zones; evidence from the high-pressure subduction mélange of New Caledonia. Contrib. Mineral. Petrol. 155, 181–198.

Straub, S.M., Layne, G.D., 2003. The systematics of chlorine, fluorine, and water in Izu arc front volcanic rocks: implications for volatile recycling in subduction zones. Geochim. Cosmochim. Acta 67 (21), 4179–4203.

Tamura, A., Arai, S., 2006. Harzburgite–dunite–orthopyroxenite suite as a record of supra-subduction zone setting for the Oman ophiolite mantle. Lithos 90, 43–56.

Tricart, P., Lemoine, M., 1983. Serpentinite oceanic bottom in South Queyras ophiolites (French Western Alps): record of the incipient oceanic opening of the Mesozoic ligurian Tethys. Eclogae Geol. Helv. 76, 611–629.

Trümpy, R., 1980. Geology of Switzerland, a guide book. Part A: an outline of the geology of Switzerland. Schweiz. Geol. Comm., Wepf and Co., Basel.

Valley, J.W., Kitchen, N., Kohn, M.J., Neindorf, C.R., Spicuzza, M.J., 1995. UWG-2, a garnet standard for oxygen isotope ratios: strategies for high precision and accuracy with laser heating. Geochim. Cosmochim. Acta 59, 5223–5231.

Vils, F., Pelletier, L., Kalt, A., Müntener, O., Ludwig, T., 2008. The lithium, boron and beryllium content of serpentinized peridotites from ODP Leg 209 (Sites 1272A and 1274A): implications for lithium and boron budgets of oceanic lithosphere. Geochim. Cosmochim. Acta 72, 5475–5504.

Vitale Brovarone, A., Beltrando, M., Malavieille, J., Giuntoli, F., Tondella, E., Groppo, C., Beyssac, O., Compagnoni, R., 2011. Inherited ocean–continent transition zones in deeply subducted terranes: insights from Alpine Corsica. Lithos 124, 273–290.

Vitale Brovarone, A., Alard, O., Beyssac, O., Martin, L., Picatto, M., 2014. Lawsonite metasomatism and trace element recycling in subduction zones. J. Metamorph. Geol. 32, 489–514.

Wedepohl, K.H., 1995. The composition of the continental crust. Geochim. Cosmochim. Acta 59, 1217–1232.

Wenner, D.B., Taylor, H.P.J., 1973. Oxygen and hydrogen isotopic studies of the serpentinization of ultramafic rocks in oceanic environments and continental ophiolite complexes. Am. J. Sci. 273, 207–239.

Wenner, D.B., Taylor, J.H.P., 1974. D/H and O^{18}/O^{16} studies of serpentinization of ultramafic rocks. Geochim. Cosmochim. Acta 38, 1255–1286.

Yeh, H.W., 1980. D/H ratios and late-stage dehydration of shales during burial. Geochim. Cosmochim. Acta 44, 341–352.

Yui, T.-F., Yeh, H.-W., Lee, C.W., 1990. A stable isotope study of serpentinization in the Fengtien ophiolite, Taiwan. Geochim. Cosmochim. Acta 54, 1417–1426.